

Z-scheme Photocatalysts for Realization of Artificial Photosynthesis (人工光合成にむけた Z スキーム光触媒)

山梨大学大学院
医工農学総合教育部
博士課程学位論文

2024 年 3 月

依田 将臣

Table of contents

Chapter 1. Introduction	- 3 -
1.1. Research background	- 3 -
1.2. Semiconductor photocatalyst	- 5 -
1.3. Previous research on visible light response	- 9 -
1.3.1. Visible light response by band structure control	- 9 -
1.3.2. Visible light response using two-step excitation reaction (Z-scheme)	- 10 -
1.3.3. Visible light response by inserting a conductive layer between catalysts	- 11 -
1.4. Application to CO ₂ reduction	- 13 -
1.5. Overview of this research	- 14 -
1.5.1. Purpose of research	- 14 -
1.5.2. Selection of H ₂ generation photocatalyst	- 15 -
1.5.3. Selection of O ₂ generating photocatalyst	- 15 -
1.5.4. Water splitting activity evaluation method	- 16 -
1.5.5. CO ₂ reduction activity evaluation method	- 16 -
Chapter 2. Water splitting by Bi ₄ V ₂ O ₁₁ /Au/ZnRh ₂ O ₄ /Au	- 17 -
2.1. The optimal ratio of Bi ₄ V ₂ O ₁₁ , ZnRh ₂ O ₄ and Au	- 17 -
2.1.1. Preparation and sample evaluation of Bi ₄ V ₂ O ₁₁ and ZnRh ₂ O ₄	- 17 -
2.1.2. Preparation and sample evaluation of Au _{com} /ZnRh ₂ O ₄	- 18 -
2.1.3. Preparation and sample evaluation of Bi ₄ V ₂ O ₁₁ /Au _{com} /ZnRh ₂ O ₄ /Au _{com}	- 19 -
2.1.4. Water splitting activity of Bi ₄ V ₂ O ₁₁ /Au _{com} /ZnRh ₂ O ₄ /Au _{com}	- 20 -
2.2. Considering miniaturization of Au	- 21 -
2.2.1. Preparation of Au _{sp}	- 21 -
2.2.2. Preparation and sample evaluation of Au _{sp} /ZnRh ₂ O ₄	- 22 -
2.2.3. Preparation and sample evaluation of Bi ₄ V ₂ O ₁₁ /Au _{sp} /ZnRh ₂ O ₄ /Au _{sp}	- 25 -
2.2.4. Water splitting activity of Bi ₄ V ₂ O ₁₁ /Au _{sp} /ZnRh ₂ O ₄ /Au _{sp}	- 30 -
2.3. Examination of Bi ₄ V ₂ O ₁₁ /Au/ZnRh ₂ O ₄ /Au compounding ratio	- 32 -
Chapter 3. CO ₂ reduction by Bi ₄ V ₂ O ₁₁ /Ag/ZnRh ₂ O ₄	- 33 -
3.1. Fabrication and sample evaluation of Bi ₄ V ₂ O ₁₁ /Ag/ZnRh ₂ O ₄	- 33 -
3.2. Selective Cu support by photodeposition on Bi ₄ V ₂ O ₁₁ /Ag/ZnRh ₂ O ₄	- 34 -
3.3. Water splitting activity and CO ₂ reduction activity of Bi ₄ V ₂ O ₁₁ /Ag/ZnRh ₂ O ₄	- 39 -
Chapter 4. Social significance and business prospects	- 42 -
4.1. Social significance	- 42 -
4.2. Business prospects	- 43 -
Chapter 5. Conclusions	- 44 -
5.1. Conclusions	- 44 -
【References】	- 45 -
【Acknowledgment】	- 47 -

Chapter 1. Introduction

1.1. Research background

The world is already heavily dependent on fossil fuels such as oil, coal, and natural gas. However, fossil fuel reserves are limited, and their use releases large amounts of carbon dioxide (CO₂). Currently, as the world's population increases and countries develop, energy issues such as global warming are expanding on a global scale. Therefore, today's affluent lifestyle still requires the consumption of large amounts of energy, and solving these problems is essential to maintaining and improving people's lives. For that reason, research on clean energy is currently being actively conducted in a wide range of fields with the aim of solving problems as an energy alternative to fossil fuels.

Among these, solar energy is attracting particular attention as a clean energy source. Sunlight continues to illuminate the earth semi-permanently, and at the same time, the amount of energy in the upper atmosphere remains almost constant at 1.37 kW/m² throughout the year, and the amount of solar energy that enters the earth every hour is 1.73×10^{17} W. Even taking into account the absorption and reflection of light by the atmospheric layers, the energy irradiated to the earth's surface per hour is greater than the energy consumed by humans in a year. If only a few percent of this solar energy could be used, it would be possible to cover almost all of humanity's energy consumption.

On the other hand, the usefulness of hydrogen (H₂) as an energy source is attracting attention. H₂ does not emit CO₂ when burned, and only water is emitted. It also has excellent long-term storage and can be used as fuel for fuel cells. Therefore, it is possible for H₂ to replace conventional fossil fuels such as gasoline and oil, as well as electricity, which is the main source of energy conversion. For this reason, projects have started around the world aimed at creating an "H₂ society," in which H₂ is widely used as a next-generation new energy resource and form of energy storage. Since H₂ hardly exists on Earth, industrial by-products are not enough to supply it in large quantities; it is necessary to add energy to hydrocarbons and water in some way to produce H₂. However, current H₂ production is mainly carried out by steam reforming ^[1], which involves reacting fossil fuels with steam, which only furthers our dependence on fossil fuels.

Therefore, as a countermeasure against global warming and the depletion of fossil fuel resources, there are high hopes for the practical application of H₂ production using photocatalysts and "artificial photosynthesis", which is a general term for CO₂ reduction technology. Although the details will be described later, artificial photosynthesis uses water as an electron source and proton source and light energy (sunlight) as an energy source, and reduces CO₂ and protons (H⁺) reduction. The CO₂ reduction reaction is a technology that can effectively utilize CO₂, a greenhouse gas that causes global warming, as a resource, reduce CO₂, and create useful chemical resources such as methane, methanol, and formic acid. On the other hand, H⁺ reduction is a H₂ production technology. In the future, compared to water electrolysis using solar cells, it will be

possible to produce both on a large scale using a simpler system that simply exposes water coated with photocatalyst powder to sunlight. Therefore, there are many expectations for its practical application.

1.2. Semiconductor photocatalyst

Figure 1.1 shows the principle of photocatalysis in semiconductors. Unlike metals, semiconductors have energy levels where electrons exist (valence band, VB), energy levels where electrons do not exist (conduction band, CB), and energy levels at the top and bottom of the valence band. There is a region (forbidden band) where sandwiched electrons cannot exist. The energy width of this forbidden band is called the band gap (E_g), and when a photon energy ($h\nu$) greater than E_g is externally applied to the semiconductor photocatalyst, the electrons existing in the valence band are excited and shift to the conduction band. At this time, the phenomenon in which electrons (e^-) in the conductor and holes (h^+) of electrons in the valence band are generated is called charge separation, and the electron-hole pairs generated by this charge separation are mainly It moves within the crystal toward the upper end of the valence band and the lower end of the conduction band while releasing thermal energy (thermal relaxation). Furthermore, electrons transferred to the material surface contribute to the reduction of the substance, and holes contribute to the oxidation of the substance. In other words, although the photocatalytic reaction is a redox reaction, the electron-hole pairs that were not involved in the redox reaction eventually recombine and return to their original state. In addition, the probability of occupation of an electron in a band is expressed by the Fermi distribution function, and the energy level (Fermi level, E_F) at which the probability of occupation by an electron is half is important when considering semiconductor photocatalysts.

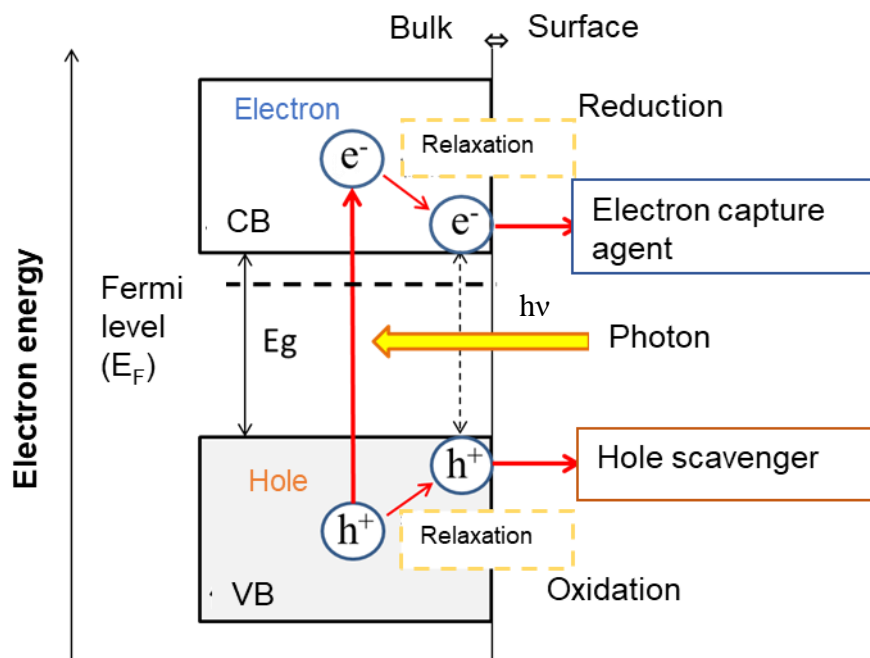


Figure 1.1. Semiconductor band structure and photocatalytic principle.

In 1972, Honda and Fujishima developed an electrochemical cell consisting of an n-type semiconductor titanium oxide (TiO_2 , rutile-type) electrode and platinum (Pt). When the TiO_2 electrode was irradiated with ultraviolet light, water electrolysis occurred. They found that the water splitting reaction progressed by applying a bias voltage of about 0.5V, which is lower than the theoretically required bias voltage (1.23V) (Figure 1.2) [2]. This phenomenon is called the "Honda-Fujishima effect" after the name of its discoverer. In this phenomenon, since TiO_2 is an n-type semiconductor, contact with the electrolyte solution forms a region (space charge layer) in which the band near the surface is bent, and when electron-hole pairs are generated by light irradiation, the electric field increases. Due to the gradient, electrons are separated into the bulk and holes are separated into the surface. After that, OH^- is oxidized on the TiO_2 surface to generate oxygen (O_2), and electrons are diffused into TiO_2 due to the electric field gradient of the space charge layer, passing through the conductive wire and generating H_2 from H^+ in Pt. The lower end potential of the conduction band of TiO_2 is more negative than the oxidation-reduction potential of H/H_2 (standard hydrogen electrode SHE: standard H electrode 0V), and the upper end potential of the valence band of TiO_2 is the oxidation potential of water (1.23 V, SHE).), which explains the mechanism. The complete decomposition reaction of water ($\text{H}_2\text{O} \rightarrow \text{H}_2 + 1/2\text{O}_2$) has a positive Gibbs free energy ($\Delta G_0 = 237 \text{ kJ/mol}$) and does not occur thermodynamically at room temperature. Therefore, this result showed that it is possible to split water using light rather than electricity and extract chemical energy in the form of H_2 . Since then, research on semiconductor photocatalysts has been actively conducted all over the world. Figure 1.3 shows the water splitting mechanism of semiconductor photocatalyst powder (model: TiO_2 , anatase-type). Since photocatalysts produce H_2 and O_2 within the catalyst, the H_2 and O_2 production potentials are more negative than the lower conduction band potential and more positive than the upper valence band potential of the photocatalytic material, respectively, depending on the thermodynamic water splitting conditions. However, actual photocatalytic water splitting reactions involve a complex interplay of factors, including lifetime, mobility, charge separation properties, overvoltage during the reaction, and the active site of the reaction due to recombination of electrons and holes generated by photoirradiation. In the TiO_2 model, the lower end of the conduction band is located near the H_2 generation potential, and the water reduction and the potential difference required to produce H_2 is small. Therefore, measures such as applying a bias voltage to the H_2 -generating side or loading a co-catalyst are necessary to obtain more H_2 production.

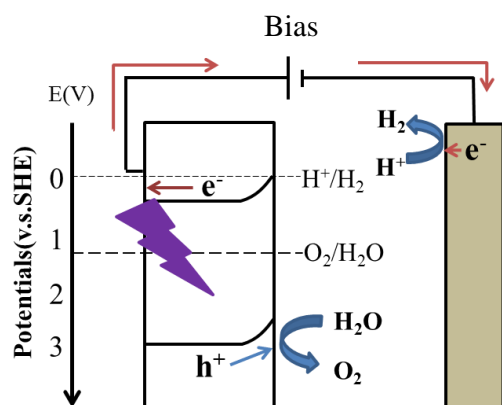


Figure 1.2. Honda-Fujishima effect.

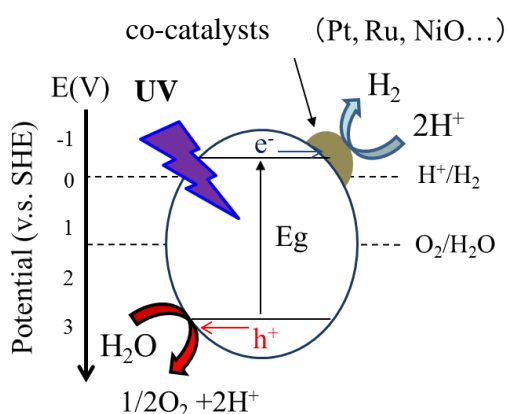


Figure 1.3. Anatase type TiO_2 photocatalytic mechanism.

Figure 1.4 shows the relationship between the band structure of various semiconductors and the redox potential of water. Photocatalysts with high conduction band levels, such as zirconium oxide (ZrO_2), can completely decompose water on their own ^[3]. However, many semiconductors satisfy the thermodynamic conditions for water decomposition, but do not proceed with the water decomposition reaction. This is because the previously mentioned factors cannot be met, and recombination of electrons and holes occurs before the reaction takes place. Therefore, recombination is often suppressed by using an auxiliary catalyst such as Pt or nickel oxide (NiO) to capture electrons and provide a reaction field ^[4-5].

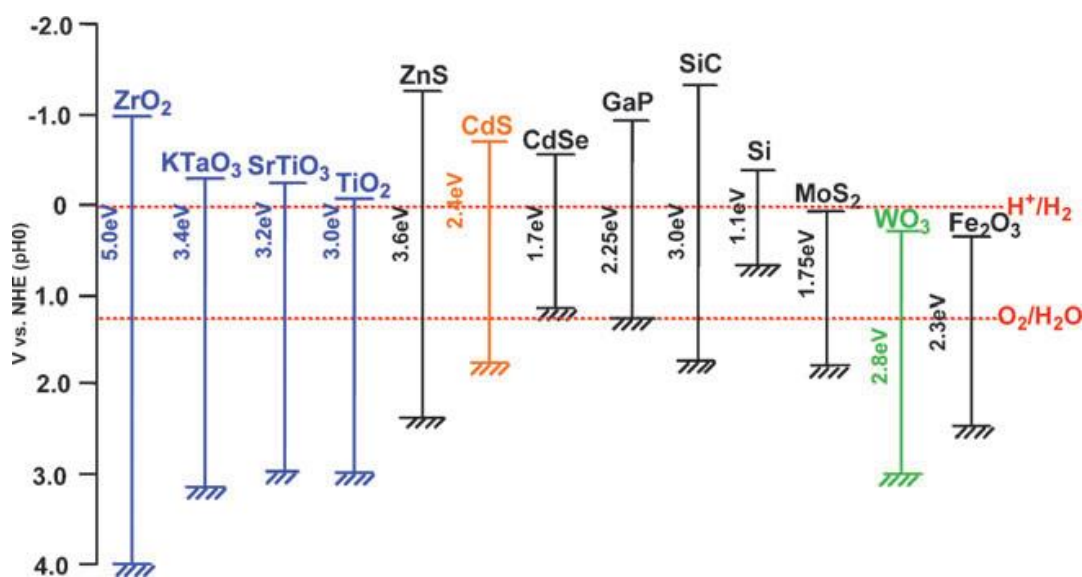


Figure 1.4. Relationship between semiconductor band structure and water redox potential.

Furthermore, there is a relationship between light energy (eV) and wavelength (λ) as in Equation (1).

$$E = 1240/\lambda \quad (1)$$

As mentioned earlier, the reaction of artificial photosynthesis occurs only when the photocatalyst absorbs photon energy above its own band gap. The shorter the wavelength of light, the higher the energy, so as can be seen from Equation (1), the larger the band gap, the shorter the wavelength of light that can be absorbed. In the previous model, the E_g of TiO_2 (anatase type) is 3.2 eV, so the wavelength is 387.5 nm from Equation (1), which means that TiO_2 absorbs only the ultraviolet region when irradiated with sunlight. However, since sunlight contains only about 3% UV light, the efficiency of sunlight utilization is low (Figure 1.5). To utilize sunlight efficiently, it is essential to use the visible light region from 380 nm ($E_g=3.2$ eV) to 760 nm ($E_g=1.6$ eV), which accounts for more than 40% of total sunlight. However, the valence band of common metal oxides consists of O 2p orbitals, and the potential is known to be about 3.0 V (vs. SHE) from Scaife's formula ^[6], and common metal oxides capable of complete water splitting have a large band gap and absorb only UV and ~400 nm visible light. Therefore, visible light sensitization of photocatalysts is essential for efficient use of solar energy and practical applications in water splitting and CO_2 reduction.

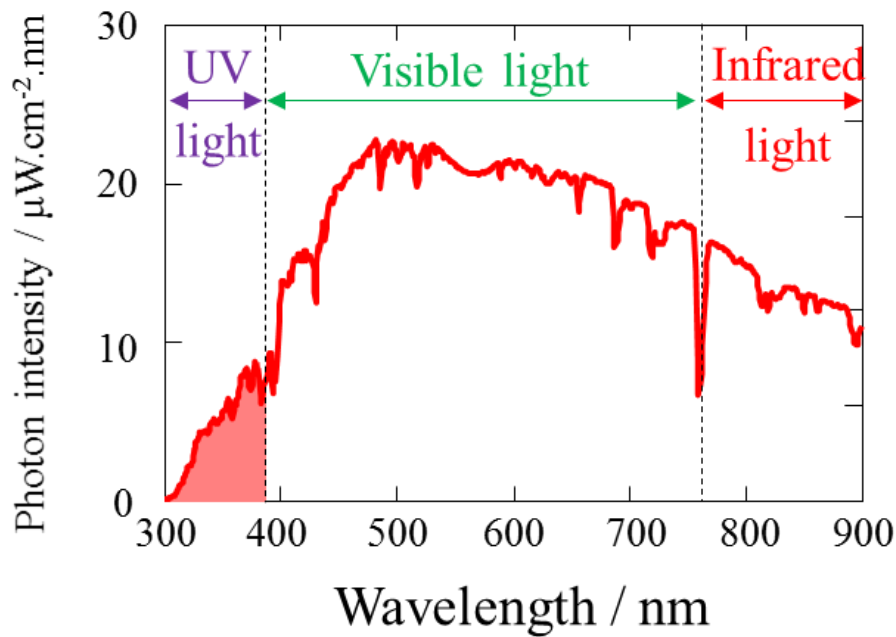


Figure 1.5. Sunlight spectrum.

1.3. Previous research on visible light response

1.3.1. Visible light response by band structure control

Controlling the band structure is one method of making photocatalysts responsive to visible light. Specifically, it can be classified into three methods shown in Figure 1.6. The first method is to respond to visible light by doping an element to form a new donor level in the forbidden band and replacing it with an O 2p orbital [1.6 (a)]. The next method is to reduce the band gap by forming mixed orbitals with O2p orbitals and Ag 4d(Ag⁺), Cu 3d(Cu⁺), Pb 6s(Pb²⁺), Bi 6s(Bi³⁺) orbitals or by forming orbitals in place of O2p orbitals [Figure 1.6 (b)]. Finally, a method in which two types of semiconductor photocatalysts are made to react to visible light by forming hybridized orbitals in the conduction band and valence band, respectively, by solid solution [Figure 1.6 (c)], thereby narrowing the band gap. To date, there have been several reports of complete water decomposition by band structure control, including a report of gallium oxide-zinc oxide (GaN-ZnO) solid solution [7-14]. More recently, Wang et al. have succeeded in water splitting at a maximum wavelength of 630 nm using yttrium titanium oxysulfide (Y₂Ti₂O₅S₂) [15]

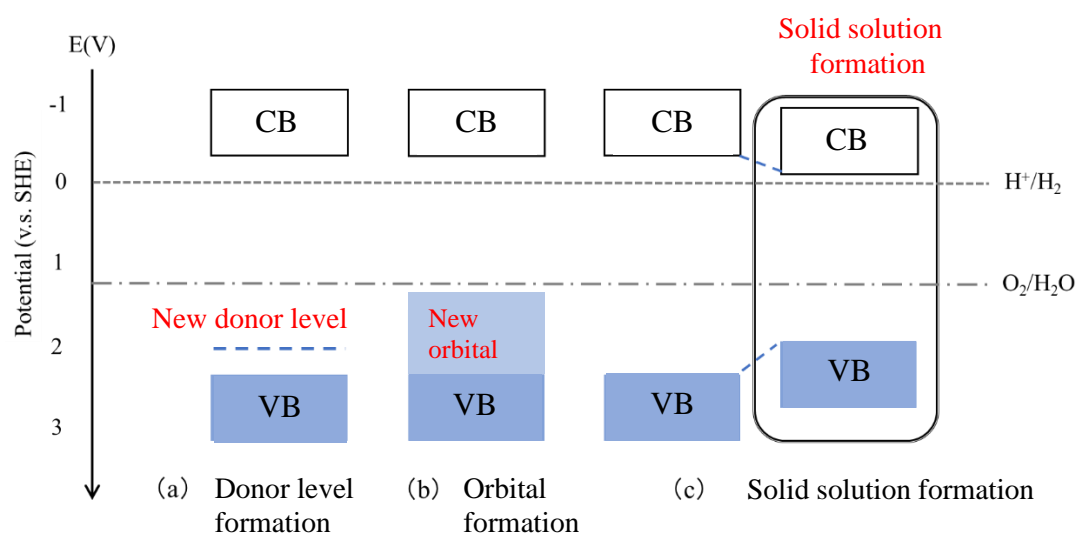


Figure 1.6. Visible light response by band structure control.

1.3.2. Visible light response using two-step excitation reaction (Z-scheme)

The lower end of the conduction band of CdSe shown in Figure 1.4 can reduce water, but the upper end of the valence band cannot oxidize water, so it cannot completely decompose water by itself. However, a photocatalyst that can generate H_2 through H^+ reduction under visible light irradiation by consuming holes by using a material that is easily oxidized (sacrificial agent) such as alcohol is called an H_2 generation photocatalyst. On the other hand, a photocatalyst that enables water oxidation under visible light irradiation by using an electron-consuming sacrificial agent such as Ag^+ or IO_3^- is called an O_2 generation photocatalyst.

Visible light response using a two-step excitation reaction (Z-scheme) combines these H_2 generation photocatalysts and O_2 generation photocatalysts to produce reversible oxidation-reduction reactions such as Fe^{2+}/Fe^{3+} . This method achieves complete water decomposition under visible light irradiation by using reversible redox ion pairs (Redox mediator) [16]. This two-step excitation system mimics plant photosynthesis. It is called an artificial photosynthesis system.

The reaction mechanism of the Z-scheme is shown in Figure 1.7. In this reaction, the H_2 generation photocatalyst is strontium titanate ($SrTiO_3$: Cr, Ta- $SrTiO_3$) doped with chromium and tantalum (Cr, Ta), and the O_2 generation photocatalyst is tungsten oxide (WO_3 : Pt- WO_3) doped with Pt. It was used in combination with an iodine-based Redox medium (I^-/IO_3^-) to achieve complete decomposition of water [16].

However, both photocatalysts must be able to redox the redox medium. Therefore, suitable photocatalyst and redox media combinations are limited. Therefore, the maximum wavelength available in this scheme system is 520 nm, with ruthenium (Ru) supported rhodium (Rh) doped $SrTiO_3$ (Ru/ $SrTiO_3$ -Rh: $E_g=2.4$ eV) as H_2 photocatalyst and bismuth vanadate ($BiVO_4$: $E_g=2.4$ eV) as O_2 photocatalysts [17].

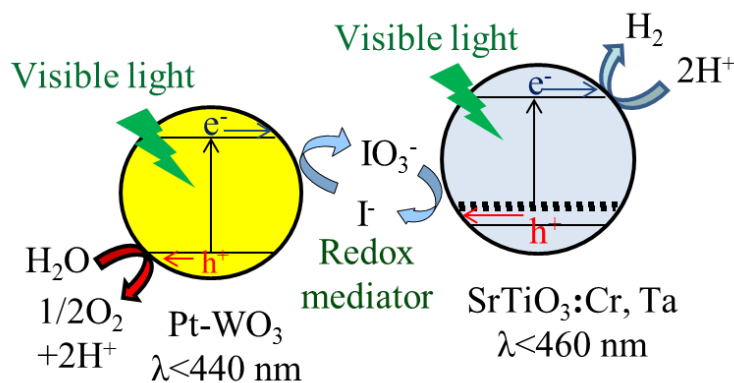


Figure 1.7. Z-scheme reaction mechanism using Redox medium. [16]

1.3.3. Visible light response by inserting a conductive layer between catalysts

The Kudo group achieved complete water splitting using visible light by introducing photoreduced graphene oxide (reduced graphene oxide: PRGO) at the interface between BiVO_4 and $\text{Rh}:\text{SrTiO}_3$ [18]. This report is based on coupling using zeta potential measurements, as well as a directly coupled system without graphene: BiVO_4 and PRGO are pre-coupled in the fabrication stage and mixed with $\text{Ru}:\text{SrTiO}_3$ -Rh in pure water [19]. The pH was then adjusted to 3.5 so that the surface charges were positively and negatively differentially charged, and they were bonded by electrostatic forces (Fig. 1.8). Furthermore, the activity was found to be more than twice that of the system prepared at pH 3.5 and bonded directly. This is because graphene acts as a conductive layer and facilitates charge transfer from the conductive band of BiVO_4 to the valence band of $\text{Ru}:\text{SrTiO}_3$ -Rh.

In 2015, the same group used TiO_2 (rutile type: $E_g=3.0$ eV) combined with RGO as a O_2 generating photocatalysts and metal sulfides such as CuGaS and CuInS_2 as H_2 generating photocatalysts in pure water without pH adjustment. After dispersion and precipitation, the pure water was completely decomposed by UV irradiation from directly above [20]. In the absence of the conductive layer, RGO, only H_2 was produced and complete water decomposition did not proceed. This is important evidence that graphene plays an important role as a conductive layer that facilitates charge exchange. Metal sulfides exhibit excellent visible light absorption properties because the S 3p orbital forms the upper end of the valence band on the negative side of the O 2p orbital, but they are limited to sacrificial H_2 generation only because they cause autoxidation due to light absorption. Reaction with sulfur atoms in metal sulfides and metal sulfides Since the turnover numbers calculated from the number of electrons are 477 and 1.8, respectively, the complete decomposition of water by the Z-scheme reaction has proceeded. Therefore, this is a very interesting finding that shows that the material selectivity of the photocatalyst can be expanded by inserting a conductive layer between the photocatalysts. Currently, this system has stability problems because some of the metal sulfide surfaces are photo-oxidized.

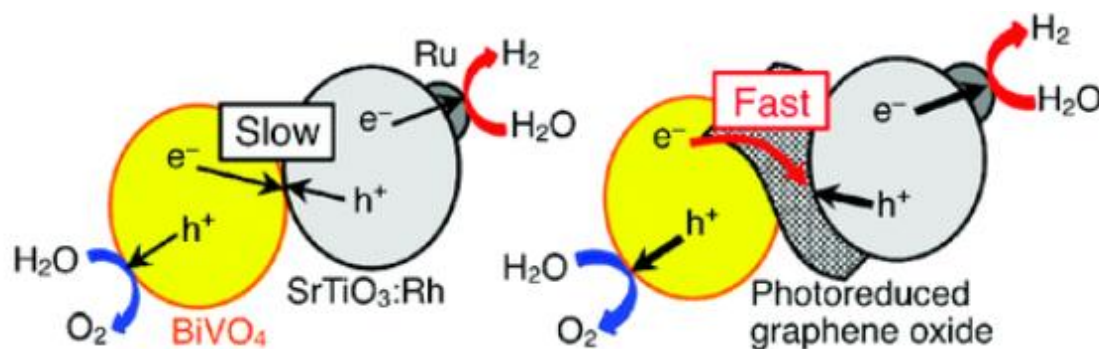


Figure 1.8. Water splitting process in $\text{BiVO}_4/\text{PRGO}/\text{Ru}:\text{SrTiO}_3\text{-Rh}$ system. [18]

In our laboratory, we have fabricated an all-solid-state Z-scheme photocatalyst that is bonded to both catalysts via a conductive layer by inserting metal particles as a conductive layer, and succeeded in completely decomposing pure water. This method is highly practical because it does not require pH adjustment or redox couple reagents, which are often used in water splitting.

Among them, bismuth vanadium oxide ($\text{Bi}_4\text{V}_2\text{O}_{11}$) was used as the O_2 -producing photocatalyst, zinc rhodium oxide (ZnRh_2O_4) as the H_2 -producing photocatalyst, and silver (Ag) and gold (Au) were inserted as conductive layers, respectively, $\text{Bi}_4\text{V}_2\text{O}_{11} / \text{Ag} / \text{ZnRh}_2\text{O}_4$ and $\text{Bi}_4\text{V}_2\text{O}_{11} / \text{Au} / \text{ZnRh}_2\text{O}_4$, successfully decomposed pure water completely in the visible light region up to 740 nm (Figure 1.9) [21-22]. These are Z-scheme photocatalysts that can satisfy both the decomposing of pure water and the broadening of the absorption range of the solar spectrum.

The bonded system with Ag shows excellent activity, but requires nitric acid treatment because the excess Ag on the surface acts as a sacrificial agent. On the other hand, Au has been reported to act as a co-catalyst for H_2 production on the ZnRh_2O_4 surface [23] and can be easily synthesized without the need to remove Au from the surface. However, since the particle size of Au is almost the same as that of ZnRh_2O_4 , the H_2 -generating photocatalyst (about 100-300 nm), it is difficult to efficiently bond $\text{Bi}_4\text{V}_2\text{O}_{11}$ and ZnRh_2O_4 using Au as a conductive layer. For higher activity, it is considered necessary to study the miniaturization of the conductive layer and the composition ratio.

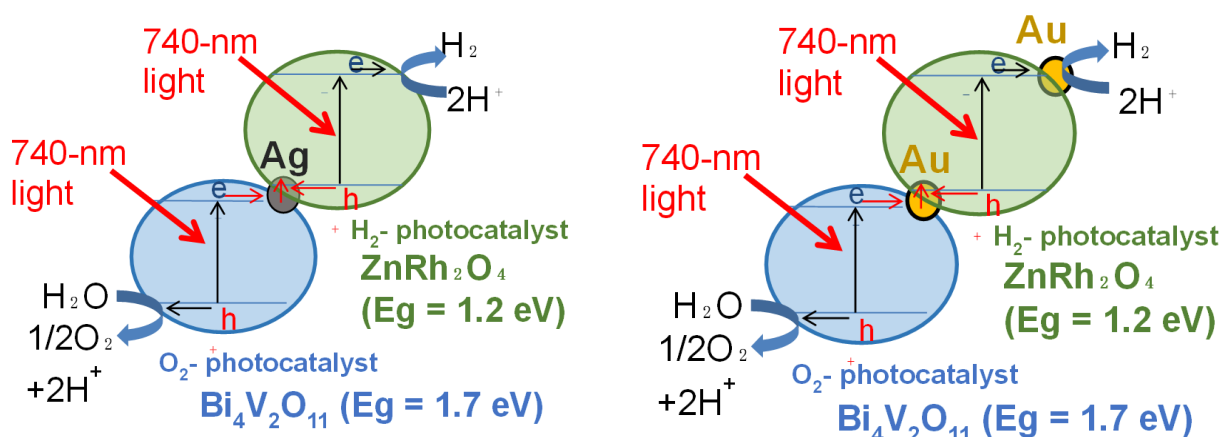


Figure 1.9. Water splitting reaction process in $\text{Bi}_4\text{V}_2\text{O}_{11} / \text{Ag}$ or $\text{Au} / \text{ZnRh}_2\text{O}_4$. [21-22]

1.4. Application to CO₂ reduction

Theoretically, the principles of CO₂ reduction and water splitting are the same and occur in the presence and absence of CO₂, respectively. The CO₂ reduction reaction proceeds in the presence of CO₂ and water, with water acting as an electron donor and proton source. In other words, the oxidation reaction of the CO₂ reduction reaction is $2\text{H}_2\text{O} + 4\text{h}^+ \rightarrow \text{O}_2 + 4\text{H}^+$, which is the same as the oxidation reaction of water splitting. On the other hand, the reduction reaction is different between water splitting and CO₂ reduction; in water decomposing, $4\text{H}^+ + 4\text{e}^- \rightarrow 2\text{H}_2$ ($\text{H}_2 \uparrow$), and in CO₂ reduction, for example $1/2\text{CO}_2 + 4\text{H}^+ + 4\text{e}^- \rightarrow 2\text{CO} + 2\text{H}_2\text{O}$ ($\text{CO} \uparrow$), $1/2\text{CO}_2 + 4\text{H}^+ + 4\text{e}^- \rightarrow 1/2\text{CH}_4 + \text{H}_2\text{O}$ ($\text{CH}_4 \uparrow$) (Figure 1.10). Therefore, in the CO₂ reduction process, multiple CO₂ reduction reactions and proton reduction reactions proceed competitively, and in order to specifically cause the desired reaction, it is common to use a co-catalyst with appropriate reduction selectivity.

Only a limited number of powdered photocatalysts that simultaneously achieve CO₂ reduction and O₂ production under visible light irradiation have been developed. For example, BiOI/g-C₃N₄ [24], nickel aluminum layered double hydroxide/g-C₃N₄ [25], various metal sulfides supporting platinum/RGO/bismuth vanadate supporting cobalt oxide [26], etc. has been reported. However, the visible light sensitivity to CO₂ reduction is still limited and has only been confirmed in experiments using light with wavelengths longer than 420 nm. In addition, the product of CO₂ reduction was mainly carbon monoxide (CO).

Our laboratory reported the possibility of reducing CO₂ using water as an electron donor and proton source using Bi₄V₂O₁₁/Au/ZnRh₂O₄ [27]. It was confirmed that this photocatalyst produced CO₂ in the presence of both CO₂ and water, and did not produce CO₂ under light irradiation in the presence of CO₂ alone. However, the light source was a full xenon (Xe) lamp, which covers the spectrum from ultraviolet to visible light. Furthermore, no occurrence of O₂ was detected. As CO₂ reduction progresses, O₂ is also generated, so simultaneous observation of CO₂ reduction by visible light irradiation and O₂ generation is an important factor in demonstrating CO₂ reduction by photocatalyst.

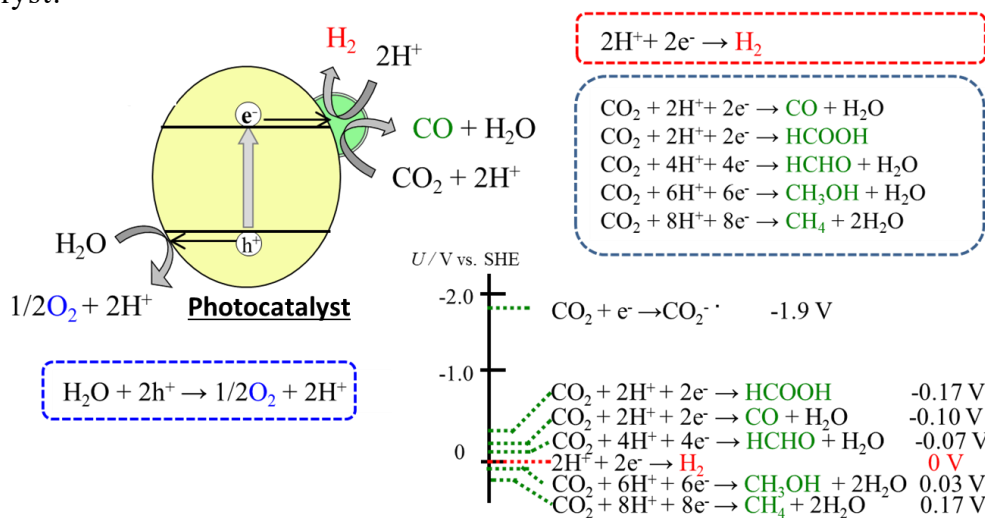


Figure 1.10. Reaction process in photocatalyst in the presence of CO₂.

1.5. Overview of this research

1.5.1. Purpose of research

In the research on visible light responsiveness described in ``Section 1.3'', the maximum wavelength used to achieve complete water decomposition as of 2023, excluding reports from this laboratory, is 630 nm for one-step excitation, and 630 nm for two-step excitation. In the excitation system, the maximum remains at 520 nm. Furthermore, as a practical goal, a photocatalyst that can stably produce a quantum yield of about 30% at 600 nm (20% quantum yield at 700 nm) is required ^[28]. If water splitting can actually be achieved with the above efficiency, this target value corresponds to an efficiency of converting sunlight to hydrogen (STH) of approximately 4% (Figure 1.11).

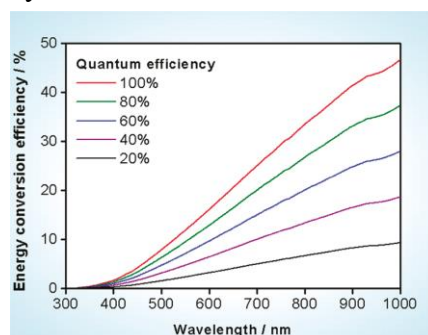
Even in our laboratory, we have not yet reached the target value for practical use in terms of quantum yield, which is a combination of research results to date (initiatives toward higher activation, such as enlarging the reaction vessel and supporting co-catalysts).

Therefore, in this study, I conducted an all-solid-state two-photon excited water splitting photocatalyst Bi₄V₂O₁₁/Au/ZnRh₂O₄/ that responds to the entire visible light range and can completely decompose pure water and generate H₂ and O₂ at a stoichiometric ratio of 2:1. By focusing on Bi₄V₂O₁₁/Au/ZnRh₂O₄/Au and Bi₄V₂O₁₁/Ag/ZnRh₂O₄, I aimed to further improve their water-splitting activity and reduction selectivity in order to commercialize future photocatalytic artificial photosynthesis technology.

In Chapter 2, using Bi₄V₂O₁₁/Au/ZnRh₂O₄/Au, I investigated (1) finding the optimal ratio of the constituent materials Bi₄V₂O₁₁, ZnRh₂O₄, and Au, and (2) the improvement of water splitting activity by making Au nanoparticles. In the first investigation, I compared the dependence of the compounding ratio of Bi₄V₂O₁₁/Au/ZnRh₂O₄/Au using Au (Au_{com}), which was used in the conventional manufacturing method, and found the optimal ratio. Using this ratio, I conducted the next investigation on Au miniaturization. Au functions as a conductive layer and a H₂ generation co-catalyst, but the particle size of Acom is about the same as that of ZnRh₂O₄ (approximately 100-300 nm), which solves the problem of not being able to bond efficiently as a conductive layer between Bi₄V₂O₁₁ and ZnRh₂O₄. By miniaturizing the Au particles used in the conductive layer, the surface area of Au increases and the number of particles increases with the same amount, making it possible to improve the efficiency of bonding using Au as a conductive layer and to uniformly distribute fine Au on the surface. I conducted my research with the idea that this would effectively function as a co-catalyst and improve water splitting activity. This study used miniaturized Au (Au_{sp}) obtained by sputtering Au into an ionic liquid ^[29].

In Chapter 3, I evaluated the CO₂ reduction activity of Bi₄V₂O₁₁/Ag/ZnRh₂O₄ by selectively supporting a copper (Cu) co-catalyst onto ZnRh₂O₄. I selected these photocatalysts because our laboratory had already conducted research on water splitting activity evaluation using Cu co-catalysts, and we had a wealth of comparative data and knowledge regarding supporting conditions. In addition, Cu was used as a reduction co-catalyst because it is known to be able to reduce CO₂ to methane (CH₄).

Figure 1.11. Calculated solar energy conversion efficiency as a function of wavelength for overall water splitting using photocatalysts with various quantum efficiencies.^[28]



1.5.2. Selection of H₂ generation photocatalyst

For the H₂ generation photocatalyst, I selected ZnRh₂O₄, which was discovered in our laboratory in 2012 [30]. The pseudo-closed-shell electronic structure ion Rh³⁺ in ZnRh₂O₄ has a d⁶ electron configuration, and its d-orbitals undergo ligand field splitting into t_{2g}-e_g in the regular octahedral crystal field (Figure 1.12). ZnRh₂O₄ consists of a t_{2g}⁶ orbital at the top of the valence band and an e_g⁰ orbital at the top of the conductor, so it has a very small band gap of approximately 1.2 eV and can respond to infrared light. Furthermore, the upper end of the valence band is ~0.1 V (vs. SHE), which is significantly more negative than that of general oxides, and the lower end of the conduction band is ~-1.1 V (vs. SHE), which is much more negative than the proton reduction potential.

In fact, in a half-reaction experiment of water using formaldehyde (HCHO) as a sacrificial agent and irradiated with monochromatic light with a wavelength of 770 nm ± 25 nm, which corresponds to the entire visible light range, H₂ was produced with extremely high quantum yield of ~27%. has been confirmed to occur (Figure 1.13).

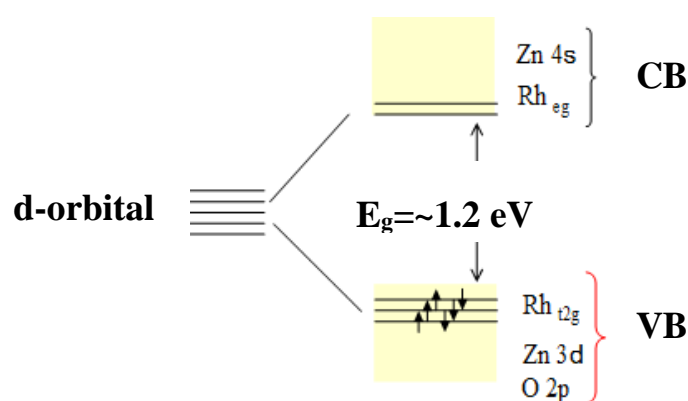


Figure 1.12. ZnRh₂O₄ band structure.

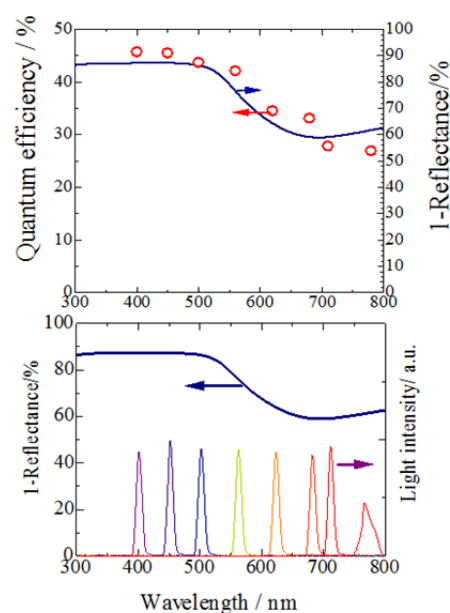


Figure 1.13. ZnRh₂O₄ hydrogen evolution action spectrum.

1.5.3. Selection of O₂ generating photocatalyst

Bi₄V₂O₁₁ is expressed by the general formula [Bi₂A_{n-1}B_nO_{3n+3}] (n=1), and has a layered structure in which a perovskite block [A_{n-1}B_nO_{3n+1}]²⁻ (n=1) is sandwiched between [Bi₂O₂]²⁺ sheets [31]. Its valence band is formed by a hybrid orbital of Bi 6s and O 2p, and the conduction band is formed by a V 3d orbital [32]. Therefore, it can be expected to have visible light responsiveness and high O₂ generation activity similar to BiVO₄, which has been reported as a highly active O₂ generation photocatalyst under visible light. However, there are only a few reports on Bi₄V₂O₁₁ as a photocatalyst [33]. Furthermore, it is not known whether it is a direct transition semiconductor or an indirect transition semiconductor, and although there are reports that it is around 2 eV based on the knowledge of BiVO₄, the exact band gap is not known. However, in 2016, our laboratory achieved complete water splitting using wavelengths up to 740 nm, so I selected Bi₄V₂O₁₁ as the O₂ generation photocatalyst that responds to red light.

1.5.4. Water splitting activity evaluation method

A dual closed circulation device for photocatalytic reactions (Makuhari Rikagaku Glass CLS-1370-PSWG) was used to evaluate water splitting activity. Figure 1.14 is a schematic diagram of an actual dual closed circulation device for photocatalytic reactions. The photocatalytic reaction was carried out in a Pyrex glass reaction vessel with a closed circulation system. Add 60 mg of photocatalyst powder and 12 mL of pure water to the reaction container, degas the air from the reaction solution, introduce Ar gas 50 kPa into the circulation system, and stir using a stirrer and a stirrer. Light irradiation was performed while stirring. An LED 700 nm (Cytec, SPL-25-DIM-CCR-50) was used for the irradiation light. The generated gas was quantitatively determined using TCD gas chromatography (Shimadzu GC-8A).

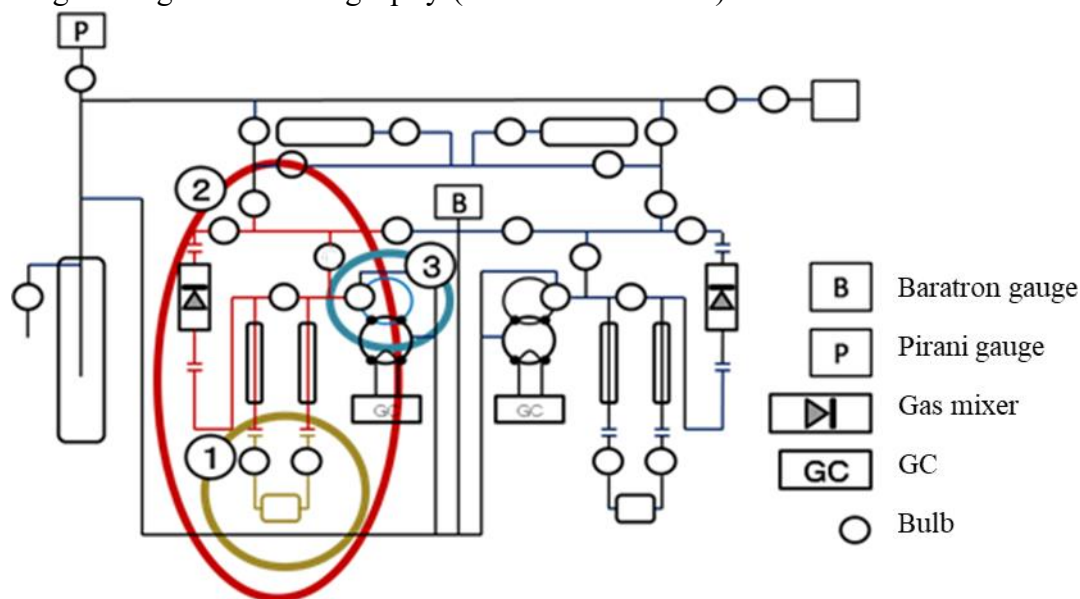


Figure 1.14. Schematic diagram of a dual closed circulation device for photocatalytic reaction. ① Reaction vessel, ② Circulation system, ③ Sampling loops.

1.5.5. CO₂ reduction activity evaluation method

In the CO₂ activity evaluation, a double closed circulation device for photocatalytic reaction was used as in the water splitting activity evaluation. However, 60 mg of photocatalyst powder and 12 mL of pure water were added to the reaction vessel, and after replacement by degassing, the respective atmospheric gases (He, ¹²CO₂, ¹³CO₂) at 50 kPa was introduced into the circulation system, and light irradiation was performed while stirring with a stirrer and a stirrer. The same LED 700 nm was used as the irradiation light source, and the CO₂ activity of the generated gas was evaluated using gas chromatograph mass spectrometer (GCMS, GCMS-QP 2010 Ultra, Shimadzu), which was operated in selective ion mode, and ions with masses of 16 (¹²CH₄), 17 (¹³CH₄), 28 (¹²C¹⁶O), 29 (¹³C¹⁶O), and 32 (¹⁶O¹⁶O) were monitored.

Chapter 2. Water splitting by $\text{Bi}_4\text{V}_2\text{O}_{11}/\text{Au}/\text{ZnRh}_2\text{O}_4/\text{Au}$

2.1. The optimal ratio of $\text{Bi}_4\text{V}_2\text{O}_{11}$, ZnRh_2O_4 and Au

2.1.1. Preparation and sample evaluation of $\text{Bi}_4\text{V}_2\text{O}_{11}$ and ZnRh_2O_4

$\text{Bi}_4\text{V}_2\text{O}_{11}$ and ZnRh_2O_4 were prepared by solid-phase method.

To prepare $\text{Bi}_4\text{V}_2\text{O}_{11}$, powders of bismuth oxide (Bi_2O_3 : Kanto Kagaku, purity 99.9%) and vanadium oxide (V_2O_5 : Kanto Kagaku, purity 99.9%) weighed in stoichiometric ratios were mixed with zirconia balls (ZrO_2 : YTZ, $\phi 5$ mm) and acetone in a polyethylene bottle, and ground and mixed for 20 h in a tabletop ball mill (V-2ML). After removing the ZrO_2 balls, the mixed sample was dried and collected using a rotary evaporator (Aira Tokyo Rika Kiki, Model N-1100S), and then placed in a mold and pressed at a pressure of 60 kN to produce pellets. The produced pellets were produced by firing in air at 850°C for 8 hours using an electric furnace. To produce ZnRh_2O_4 , zinc oxide (ZnO : Kanto Kagaku, purity 99.0%) and rhodium oxide (Rh_2O_3 : Kanto Kagaku, purity 99.9%) are used as starting materials, and powders weighed in stoichiometric ratios are mixed with ZrO_2 balls and ethanol. The mixture was placed in a polyethylene bottle and ground and mixed in a ball mill for 20 hours. After removing the ZrO_2 balls, the mixed sample was dried and collected using a rotary evaporator, and then placed in a mold and pressed at a pressure of 60 kN to produce pellets. The produced pellets were produced by firing in air at 1150°C for 24 hours using an electric furnace.

The prepared $\text{Bi}_4\text{V}_2\text{O}_{11}$ and ZnRh_2O_4 powders were evaluated by X-ray diffraction analysis (XRD PHILIPS, PW-1729) and ultraviolet-visible (UV-Vis) diffuse reflectance spectroscopy (V-650, JASCO). In this UV-Vis diffuse reflectance spectrum measurement, barium sulfate (BaSO_4) was used as a standard sample for reflectance.

The XRD pattern of the prepared $\text{Bi}_4\text{V}_2\text{O}_{11}$ powder is shown in Figures 2.1-2.2. A single phase of $\text{Bi}_4\text{V}_2\text{O}_{11}$ and ZnRh_2O_4 was confirmed from the XRD pattern. The results of the UV-Vis diffuse reflectance spectrum are summarized in Figure 2.5. As a result, I confirmed that the photocatalyst absorbs light in the entire visible light range.

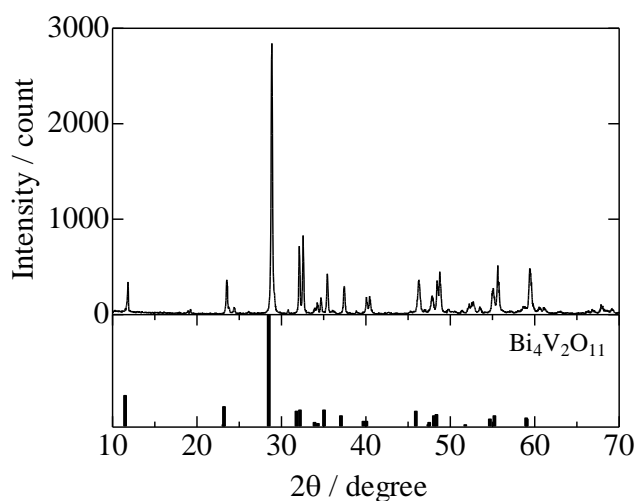


Figure 2.1. XRD pattern of $\text{Bi}_4\text{V}_2\text{O}_{11}$.

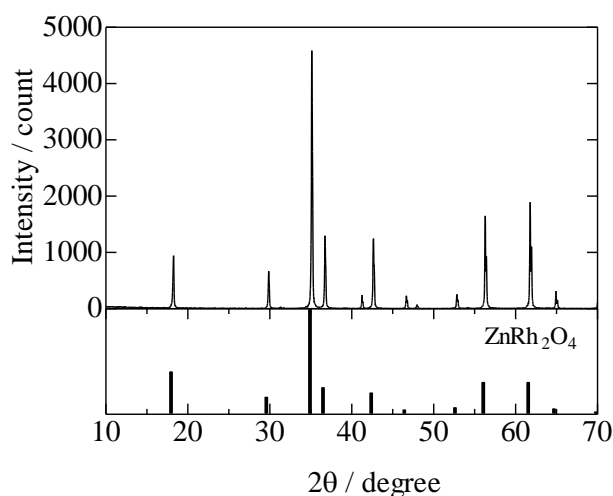


Figure 2.2. XRD pattern of ZnRh_2O_4 .

2.1.2. Preparation and sample evaluation of $\text{Au}_{\text{com}}/\text{ZnRh}_2\text{O}_4$

Since Au functions as a H_2 generation co-catalyst, it was first bonded with ZnRh_2O_4 . $\text{Au}_{\text{com}}/\text{ZnRh}_2\text{O}_4$ was prepared by solid phase method. To produce $\text{Au}_{\text{com}}/\text{ZnRh}_2\text{O}_4$, Au_{com} (ARUDRICH, purity: 99.9%, Au_{com}) and ZnRh_2O_4 powder prepared in advance were weighed according to the compounding ratio, placed in a polyethylene bottle together with ZrO_2 balls and ethanol, and mixed for 20 hours. After removing the zirconia balls, the mixed sample was dried and collected using a rotary evaporator, and then placed in a mold and pressed at a pressure of 60 kN to produce pellets. The produced pellets were produced by firing in air at 850°C for 2 hours using an electric furnace.

Figure 2.3 shows the XRD pattern of the prepared $\text{Au}_{\text{com}}/\text{ZnRh}_2\text{O}_4$ powder. Au and ZnRh_2O_4 were confirmed from the XRD pattern.

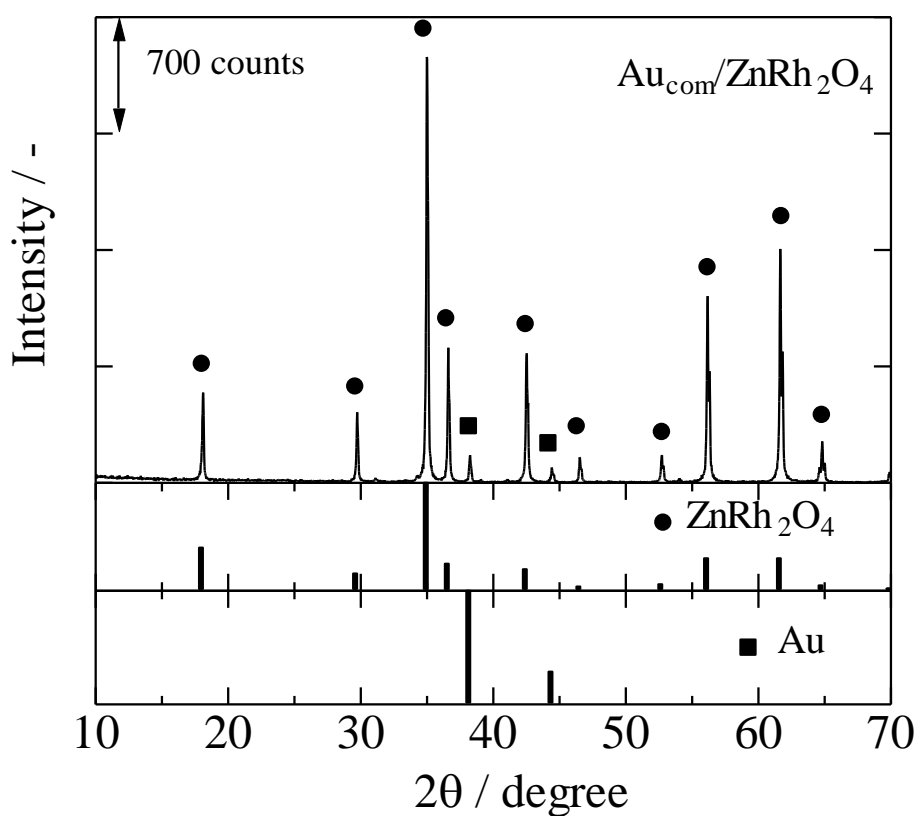


Figure 2.3. XRD pattern of $\text{Au}_{\text{com}}/\text{ZnRh}_2\text{O}_4$ (0.15: 1 mol)

2.1.3. Preparation and sample evaluation of $\text{Bi}_4\text{V}_2\text{O}_{11}/\text{Au}_{\text{com}}/\text{ZnRh}_2\text{O}_4/\text{Au}_{\text{com}}$

$\text{Bi}_4\text{V}_2\text{O}_{11}/\text{Au}_{\text{com}}/\text{ZnRh}_2\text{O}_4/\text{Au}_{\text{com}}$ was prepared by solid phase method. To prepare $\text{Bi}_4\text{V}_2\text{O}_{11}/\text{Au}_{\text{com}}/\text{ZnRh}_2\text{O}_4/\text{Au}_{\text{com}}$, the pre-prepared $\text{Bi}_4\text{V}_2\text{O}_{11}$ and $\text{Au}_{\text{com}}/\text{ZnRh}_2\text{O}_4$ powders were weighed according to the compounding ratio, and mixed for 4 hours by acetone wet mixing without adding ZrO_2 balls and pelletized. After that, it was baked in air at 850°C for 2 hours. Also, the reason why ZrO_2 balls were not added during the mixing process was to avoid breaking the $\text{Au}_{\text{com}}/\text{ZnRh}_2\text{O}_4$ bond.

The XRD pattern of the prepared $\text{Bi}_4\text{V}_2\text{O}_{11}/\text{Au}_{\text{com}}/\text{ZnRh}_2\text{O}_4/\text{Au}_{\text{com}}$ powder is shown in Figure 2.4. It was confirmed from the XRD pattern that the three phases were $\text{Bi}_4\text{V}_2\text{O}_{11}$, Au_{com} , ZnRh_2O_4 , respectively.

Figure 2.5 shows the results of a comparative evaluation of $\text{Bi}_4\text{V}_2\text{O}_{11}$, Au_{com} , ZnRh_2O_4 , $\text{Au}_{\text{com}}/\text{ZnRh}_2\text{O}_4$, and $\text{Bi}_4\text{V}_2\text{O}_{11}/\text{Au}_{\text{com}}/\text{ZnRh}_2\text{O}_4/\text{Au}_{\text{com}}$ using UV-Vis diffuse reflectance spectroscopy measurements. It was confirmed from the UV-Vis diffuse reflection spectrum that the photocatalyst had sufficient absorption in the visible light region, and the absorption of the final Z-scheme photocatalyst was confirmed to be similar to the peak of ZnRh_2O_4 , which has a large compounding ratio.

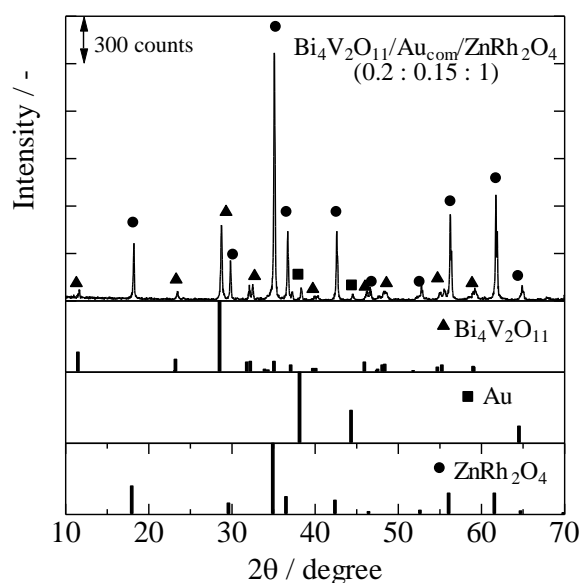


Figure 2.4. XRD pattern of $\text{Bi}_4\text{V}_2\text{O}_{11}/\text{Au}_{\text{com}}/\text{ZnRh}_2\text{O}_4/\text{Au}_{\text{com}}$ (0.2 : 0.15 : 1 mol)

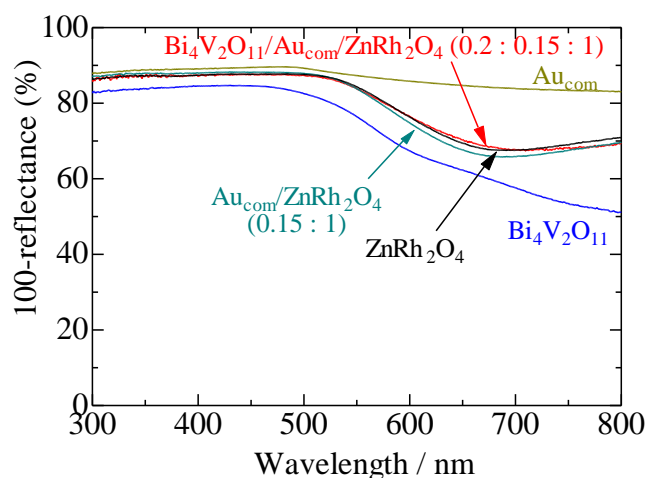


Figure 2.5. UV-vis diffuse reflectance spectrum of $\text{Bi}_4\text{V}_2\text{O}_{11}$, Au_{com} , ZnRh_2O_4 , $\text{Au}_{\text{com}}/\text{ZnRh}_2\text{O}_4$, $\text{Bi}_4\text{V}_2\text{O}_{11}/\text{Au}_{\text{com}}/\text{ZnRh}_2\text{O}_4/\text{Au}_{\text{com}}$

2.1.4. Water splitting activity of $\text{Bi}_4\text{V}_2\text{O}_{11}/\text{Au}_{\text{com}}/\text{ZnRh}_2\text{O}_4/\text{Au}_{\text{com}}$

Figures 2.6-8 summarize the apparent quantum efficiency (AQE) of samples in which complete water decomposition in pure water was confirmed by varying the $\text{Bi}_4\text{V}_2\text{O}_{11}/\text{Au}/\text{ZnRh}_2\text{O}_4$ compounding ratio. Those plots the AQE determined from the water-splitting activity on the vertical axis, and the XPS quantitative results as quantitative values (mol) on the horizontal axis. Here, AQE was calculated using the following formula from the number of photons irradiated by the light source used and the rate of H_2 generation.

$$\text{AQE} = (100 \times 4 \times \text{H}_2 \text{ generation rate}) / \text{Irradiation photon number}$$

As a result, the best activity was shown when $\text{Bi}_4\text{V}_2\text{O}_{11}/\text{Au}/\text{ZnRh}_2\text{O}_4 = 0.2/0.15/1$ mol. In order to confirm this reproducibility, I produced and measured it again, and it showed particularly high activity with an AQE of 0.051%, so I believe that the optimal compounding ratio at this point is 0.2: 0.15: 1 mol.

In the next investigation of Au miniaturization, only the amount of Au_{sp} supported was changed at a ratio of $\text{Bi}_4\text{V}_2\text{O}_{11}/\text{Au}/\text{ZnRh}_2\text{O}_4 = 0.2/x/1$ mol.

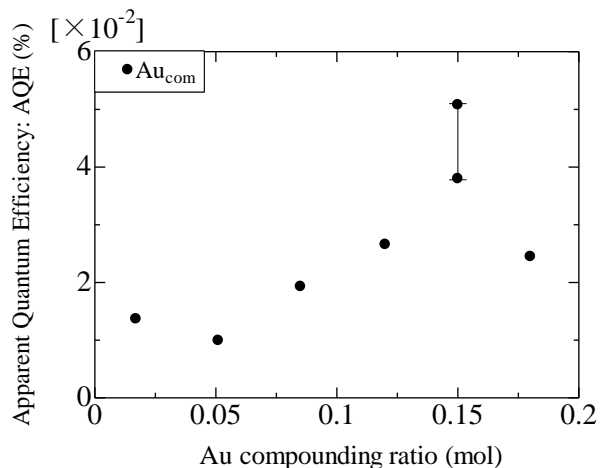


Figure 2.6. AQE comparison of $\text{Bi}_4\text{V}_2\text{O}_{11}/\text{Au}_{\text{com}}/\text{ZnRh}_2\text{O}_4/\text{Au}_{\text{com}}$ ($\text{Bi}_4\text{V}_2\text{O}_{11}$: Au: $\text{ZnRh}_2\text{O}_4 = 0.2$: x: 1 mol)

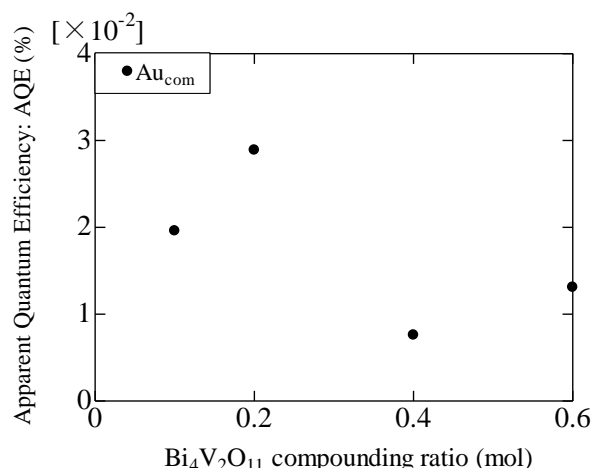


Figure 2.7. AQE comparison of $\text{Bi}_4\text{V}_2\text{O}_{11}/\text{Au}_{\text{com}}/\text{ZnRh}_2\text{O}_4/\text{Au}_{\text{com}}$ ($\text{Bi}_4\text{V}_2\text{O}_{11}$: Au: $\text{ZnRh}_2\text{O}_4 = x$: 0.12: 1 mol)

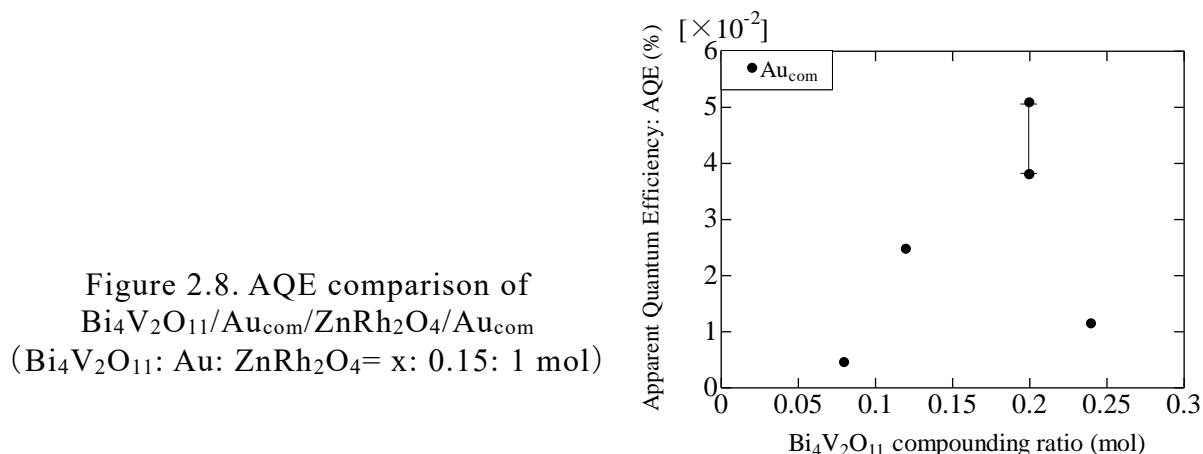


Figure 2.8. AQE comparison of $\text{Bi}_4\text{V}_2\text{O}_{11}/\text{Au}_{\text{com}}/\text{ZnRh}_2\text{O}_4/\text{Au}_{\text{com}}$ ($\text{Bi}_4\text{V}_2\text{O}_{11}$: Au: $\text{ZnRh}_2\text{O}_4 = x$: 0.15: 1 mol)

2.2. Considering miniaturization of Au

2.2.1. Preparation of Au_{sp}

Au_{sp} were fabricated by sputter deposition. Sputter evaporation is mainly used as a thin film production technique. A high voltage is applied to a metal target according to the desired film, and ionized inert gas (Ar) is applied to knock out the atoms on the target surface. It adheres and deposits on the surface. However, in the current production process, metal particles can be easily produced by sputtering the ionic liquid instead of the substrate. In order to remove residual moisture and air from the ionic liquid, *N*-methyl-*N*-propylpiperidinium bis(trifluoromethanesulfonyl) imide (PP13-TFSA: Kanto Chemical), I used a hot stirrer [Koike Precision Instruments Co., Ltd.], an aluminum block type stirrer (high temperature compatible type)] was heated and stirred at 110°C for 1 hour for pretreatment. This is to prevent bumping of the ionic liquid during Ar substitution. In addition, pre-sputtering was performed for 30 s using a sputtering device (Sanyu Electronics, SC-701HMC II) under the same conditions as the main sputtering {Au target, Ar atmosphere, evaporation current: 20 mA, sputtering pressure: 3.0 Pa} to clean the target surface. After that, the pretreated ionic liquid was added to the watch glass that had been washed with pure water, and sputtering was performed for 1 h under the same sputtering conditions to create Au_{sp}. The method for producing Au_{sp} and supporting Au_{sp} using sputter evaporation is a joint research project with the Torimoto laboratory at Nagoya University, and I began my research after learning this method from Professor Torimoto^[30]. In addition, the concentration of Au_{sp} obtained in the ionic liquid by this method is calculated from the absorbance, and the particle size (average Particle size: 2.3 nm (Figure 2.9) was confirmed through preliminary experiments at Torimoto's laboratory.

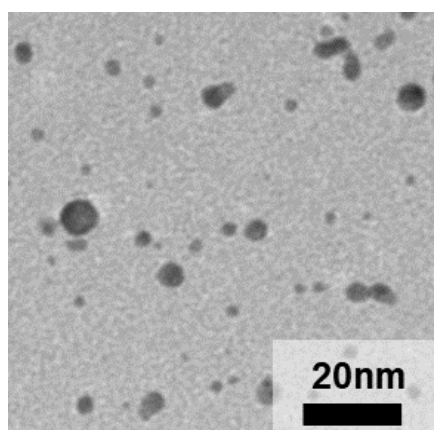


Figure 2.9. TEM image of Au_{sp}

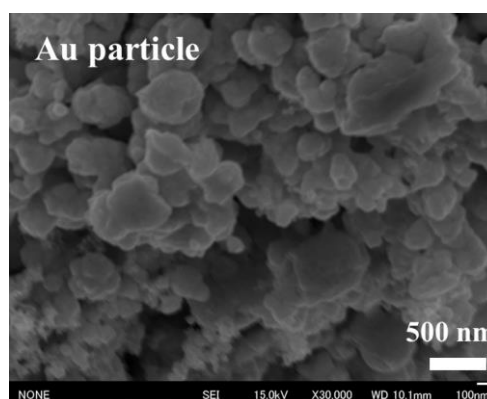


Figure 2.10. SEM image of Au_{com}^[22]

2.2.2. Preparation and sample evaluation of $\text{Au}_{\text{sp}}/\text{ZnRh}_2\text{O}_4$

An appropriate amount of Au_{sp} -containing PP13-TFSI was mixed with 140 mg of ZnRh_2O_4 (0.017, 0.085, 0.12, 0.15, 0.24 mol per 1 mol of ZnRh_2O_4 , respectively). Au_{sp} was supported on ZnRh_2O_4 by heating and stirring each mixture in a test tube at 280°C for 1 h while stirring under a nitrogen atmosphere (Figure 2.11). Then, to remove the ionic liquid from the supported sample, it was transferred to a 50 ml centrifuge tube, approximately 10 ml of acetonitrile (CH_3CN : Kanto Kagaku, purity 99.5%) was added, centrifuged at 4000 rpm for 5 min, and the supernatant removed three times in total. Thereafter, the obtained precipitate was dried into pellets and calcined in air at 850°C for 2 hours to produce $\text{Au}_{\text{sp}}/\text{ZnRh}_2\text{O}_4$. Preliminary experiments in Torimoto's laboratory confirmed that the particle size of Au_{sp} after being supported increased upon heating (average particle size: 9.0 nm) (Figure 2.12).

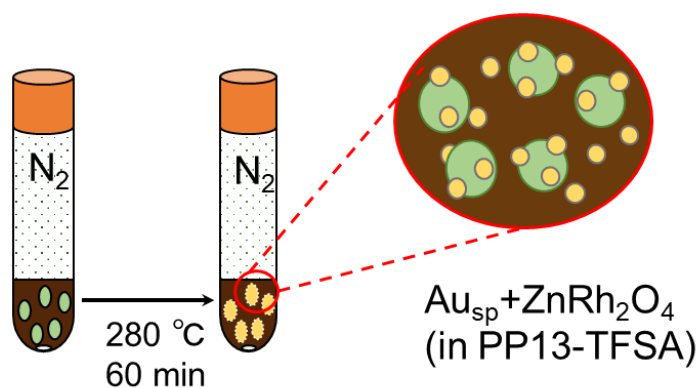


Figure 2.11. Au_{sp} support method by heating and stirring

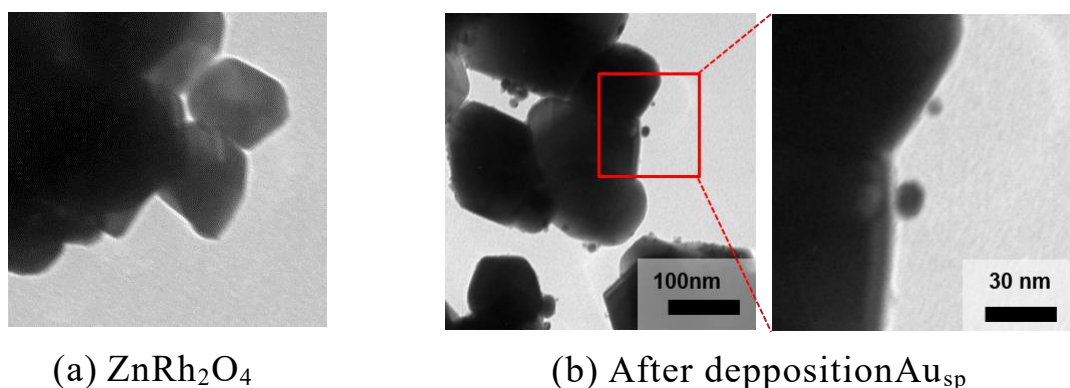


Figure 2.12. TEM image of Au_{sp} and ZnRh_2O_4 after deposition

The XRD pattern of $\text{Au}_{\text{sp}}/\text{ZnRh}_2\text{O}_4$ is shown in Figure 2.13. From the XRD pattern, it was confirmed that the Au peak increased depending on the compounding ratio.

Figure 2.14 compares the UV-Vis diffuse reflectance spectra of $\text{Au}_{\text{sp}}/\text{ZnRh}_2\text{O}_4$ samples. No trends or differences at the absorption edge could be confirmed from the UV-Vis diffuse reflectance spectra.

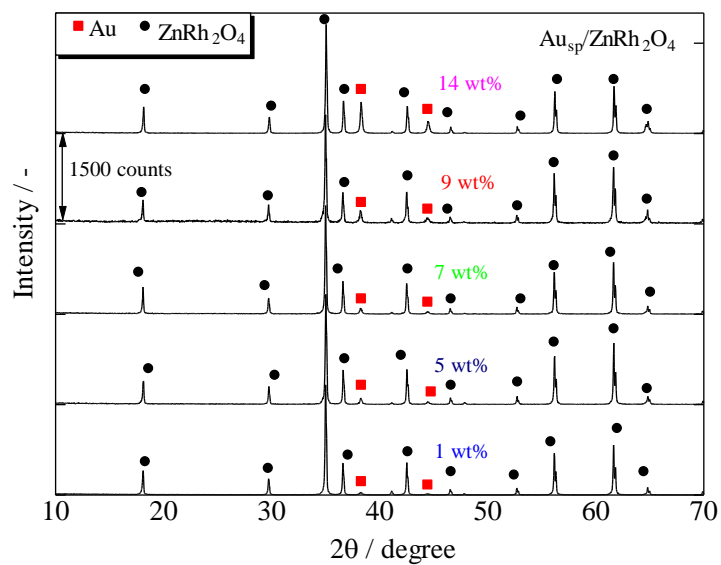


Figure 2.13. Comparison of XRD patterns of $\text{Au}_{\text{sp}}/\text{ZnRh}_2\text{O}_4$

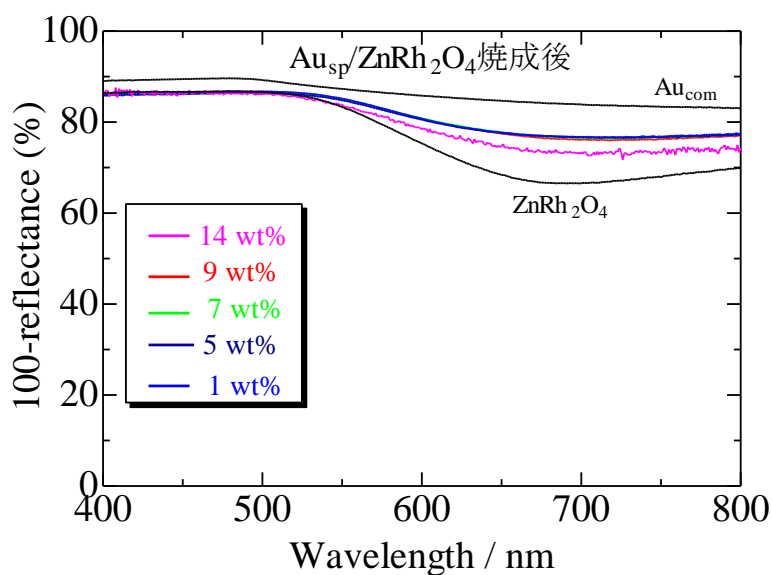


Figure 2.14. Comparison of UV-Vis diffuse reflectance spectra of $\text{Au}_{\text{sp}}/\text{ZnRh}_2\text{O}_4$

Figure 2.15 shows a SEM image of the bonded Au_{sp} . I confirmed the existence of Au_{sp} with a particle size of approximately 30-50 nm, which is smaller than the particle size of Au_{com} used so far (Figure 2.10, 100 nm-500 nm) [22]. Furthermore, as a result of determining the particle size distribution of Au_{sp} in detail from multiple TEM images, it was confirmed that the average particle size (d_{av}) was 27 nm and the standard deviation (σ) was 12 nm, as shown in Figure 2.16.

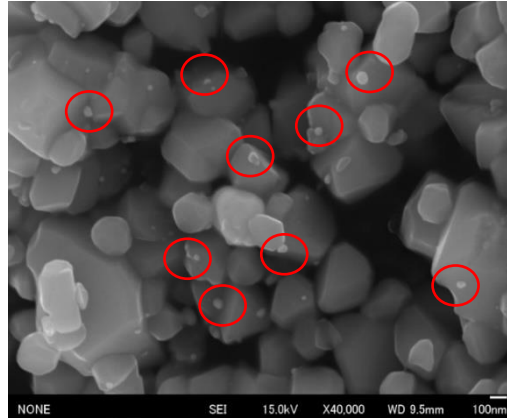


Figure 2.15. SEM image of $\text{Au}_{\text{sp}}/\text{ZnRh}_2\text{O}_4$ (Au: 9 wt%)

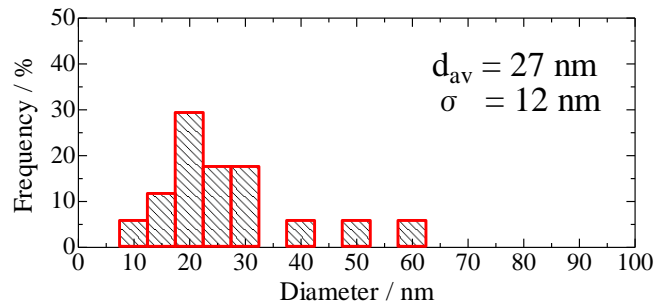


Figure 2.16. Particle size distribution of $\text{Au}_{\text{sp}}/\text{ZnRh}_2\text{O}_4$ (Au: 9 wt%)

2.2.3. Preparation and sample evaluation of $\text{Bi}_4\text{V}_2\text{O}_{11}/\text{Au}_{\text{sp}}/\text{ZnRh}_2\text{O}_4/\text{Au}_{\text{sp}}$

$\text{Bi}_4\text{V}_2\text{O}_{11}/\text{Au}_{\text{sp}}/\text{ZnRh}_2\text{O}_4/\text{Au}_{\text{sp}}$ was prepared by solid-phase method. To prepare $\text{Bi}_4\text{V}_2\text{O}_{11}/\text{Au}_{\text{sp}}/\text{ZnRh}_2\text{O}_4/\text{Au}_{\text{sp}}$, the previously prepared $\text{Bi}_4\text{V}_2\text{O}_{11}$ and $\text{Au}/\text{ZnRh}_2\text{O}_4$ powders were weighed so that $\text{Bi}_4\text{V}_2\text{O}_{11}:\text{ZnRh}_2\text{O}_4 = 0.2:1$ and were added to the acetone without adding zirconia balls. After mixing and pelletizing by wet mixing for 4 hours, the pellets were baked in air at 850°C for 2 hours. Also, the reason why zirconia balls were not added during the mixing process was to avoid breaking the $\text{Au}/\text{ZnRh}_2\text{O}_4$ bond.

The results of comparing the obtained $\text{Bi}_4\text{V}_2\text{O}_{11}/\text{Au}_{\text{sp}}/\text{ZnRh}_2\text{O}_4/\text{Au}_{\text{sp}}$ and the comparative sample ($\text{Bi}_4\text{V}_2\text{O}_{11}/\text{Au}_{\text{sp}}/\text{ZnRh}_2\text{O}_4/\text{Au}_{\text{sp}}$) using XRD patterns and UV-Vis diffuse reflectance spectra are shown in Figures 2.17-2.18. From the XRD pattern, it was confirmed that the three phases were $\text{Bi}_4\text{V}_2\text{O}_{11}$, Au and ZnRh_2O_4 , respectively. Further, no impurities were confirmed.

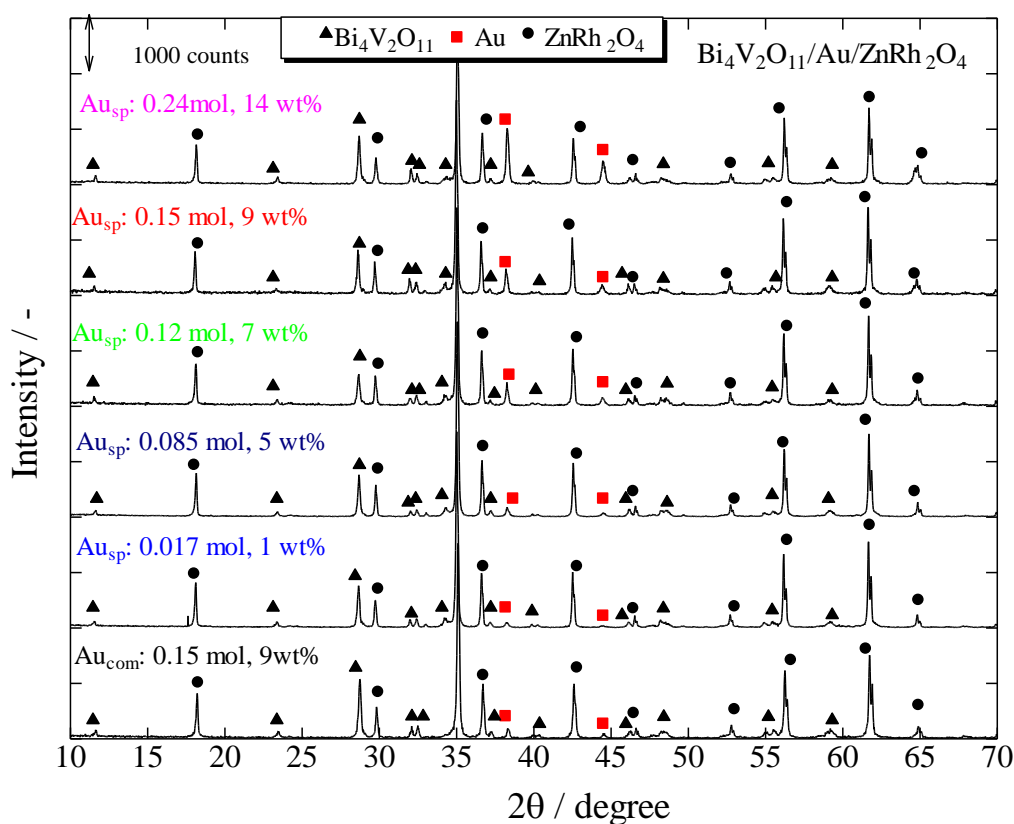


Figure 2.17. Comparison of $\text{Bi}_4\text{V}_2\text{O}_{11}/\text{Au}_{\text{sp}}/\text{ZnRh}_2\text{O}_4/\text{Au}_{\text{sp}}$ by XRD pattern

An increase in absorption due to bonding was confirmed from the UV-Vis diffuse reflectance spectrum. Moreover, at all compounding ratios, it increased significantly on the long wavelength side compared to the conventional final bonded sample. I consider that this may be due to Au_{sp} surface plasmon resonance, which absorbs wavelengths depending on particle size and shape, and this may be the cause of long-wavelength light absorption. In addition, as a result of determining the particle size distribution from multiple TEM images, it was found that the average particle size (d_{av}) was 42 nm and the standard deviation (σ) was 22 nm, as shown in Figure 2.19. As a result, I was able to achieve grain size reduction to at least one-tenth that of conventional final bonded samples.

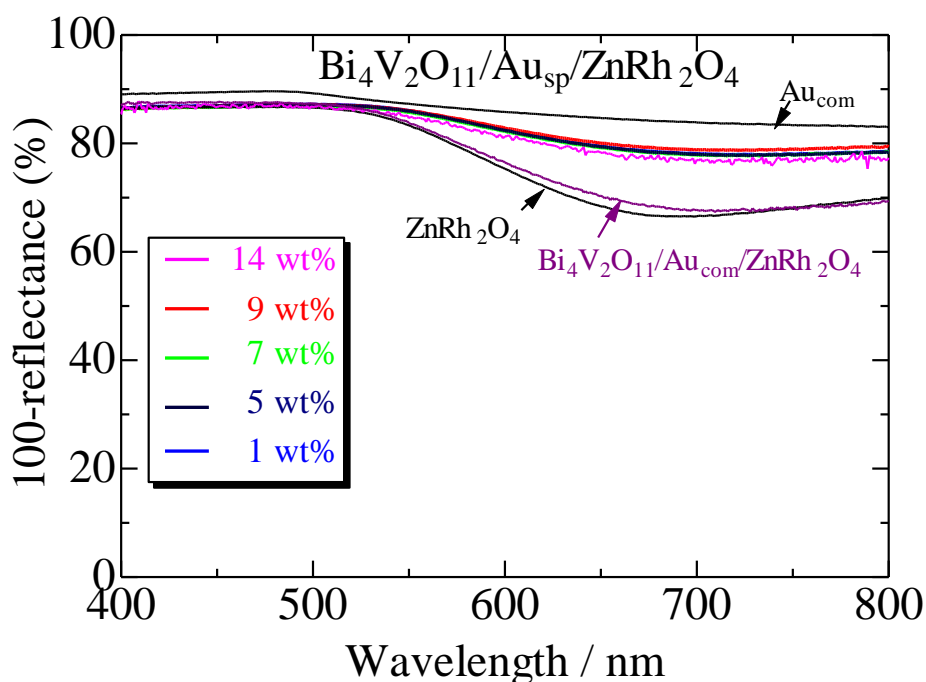


Figure 2.18. Comparison of UV-Vis diffuse reflectance spectra of $\text{Bi}_4\text{V}_2\text{O}_{11}/\text{Au}_{\text{sp}}/\text{ZnRh}_2\text{O}_4/\text{Au}_{\text{sp}}$

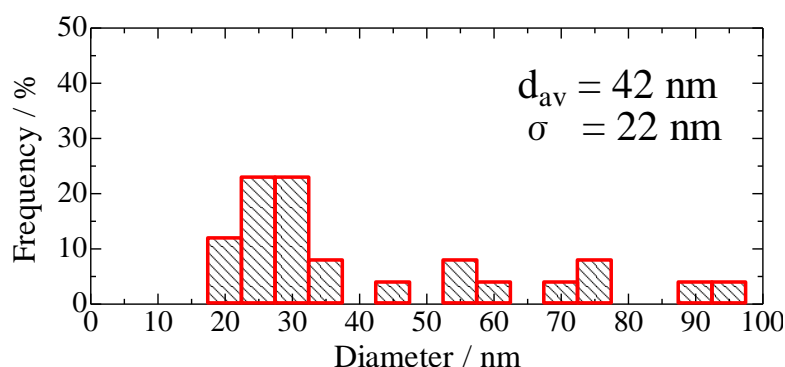
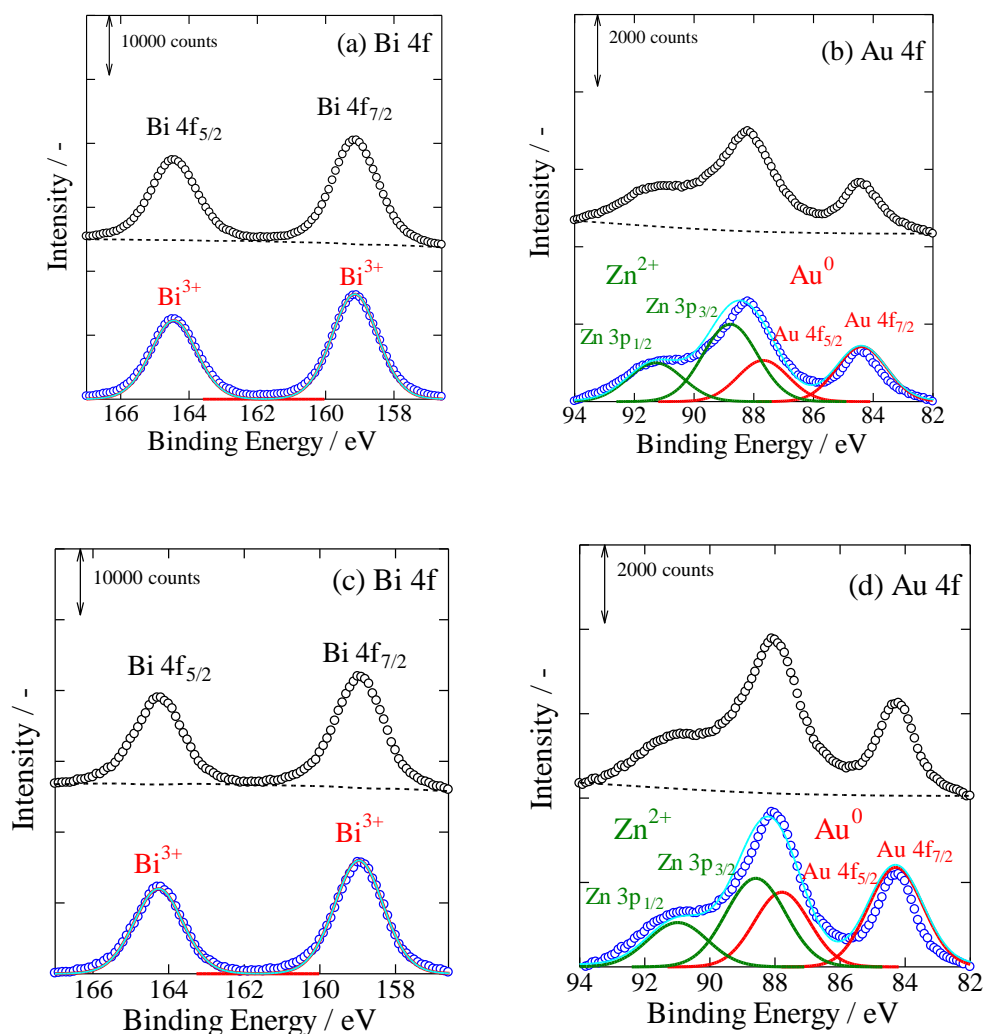


Figure 2.19. Particle size distribution of $\text{Bi}_4\text{V}_2\text{O}_{11}/\text{Au}_{\text{sp}}/\text{ZnRh}_2\text{O}_4/\text{Au}_{\text{sp}}$ (Au: 9 wt%)

As a means of quantifying the amount of Au, measurements were performed using X-ray photoelectron spectroscopy (XPS; Axis-Ultra, Shimadzu). The obtained peaks were calibrated using the C 1s peak originating from a hydrocarbon surface contaminant with a binding energy of 284.5 eV. The peak-separated 1-14 wt% results are shown in Figure 2.20, and the Au 4f peaks are summarized after peak intensity correction to match the area of the Bi 4f peak, which is considered to be least affected by surface changes. The result is shown in Figure 2.21. As a prerequisite for the quantification procedure, the ratio of the Bi 4f peak of $\text{Bi}_4\text{V}_2\text{O}_{11}$ and the Zn 3p peak of ZnRh_2O_4 , which are present in a common proportion in all samples, is unified for each sample, and the quantification of Au is determined from the ratio of the Au 4f peak to the Bi 4f peak.



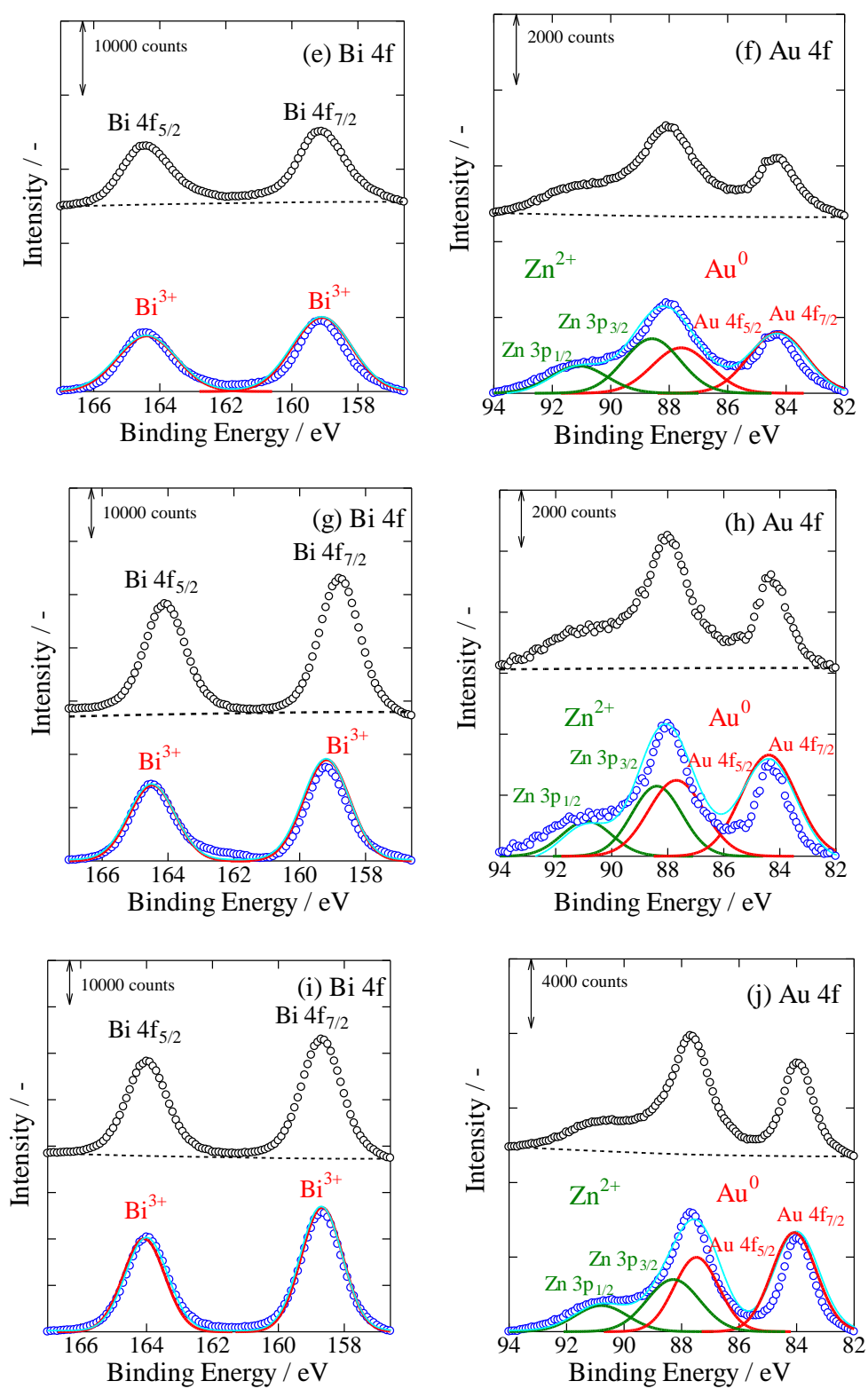


Figure 2.20. XPS spectrum peak separation results

(a) (b) 1 wt% (c) (d) 5 wt% (e) (f) 7 wt%
 (g) (h) 9 wt% (i) (j) 14 wt%

From Figure 2.22, it was confirmed that the AQE of Au_{sp} suddenly increased as the loading amount increased. This is thought to be because up to Au : 0.12 mol, the amount of Au was extremely small as a conductive layer, so it did not function well and had low activity, but as the amount of Au supported increased, it began to function as a conductive layer and became active. With the current fabrication procedure, ~ 0.3 mol is the limit for maintaining uniformity in fabrication between samples, so 0.27 mol (~ 10 wt% vs. 1 mol ZnRh_2O_4 + 0.2 mol $\text{Bi}_4\text{V}_2\text{O}_{11}$) is the maximum activity for miniaturization.

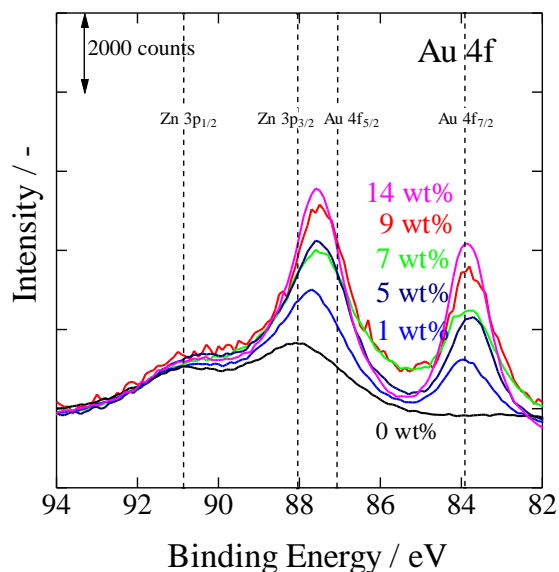


Figure 2.21. Summary of XPS spectra of $\text{Bi}_4\text{V}_2\text{O}_{11}/\text{Au}_{\text{sp}}/\text{ZnRh}_2\text{O}_4/\text{Au}_{\text{sp}}$

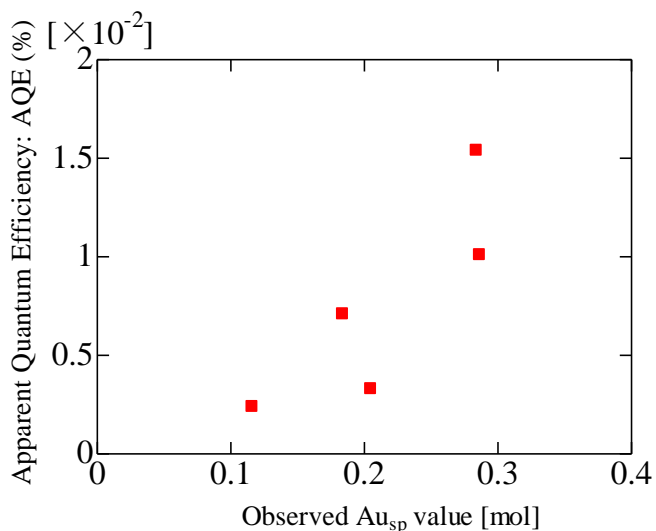
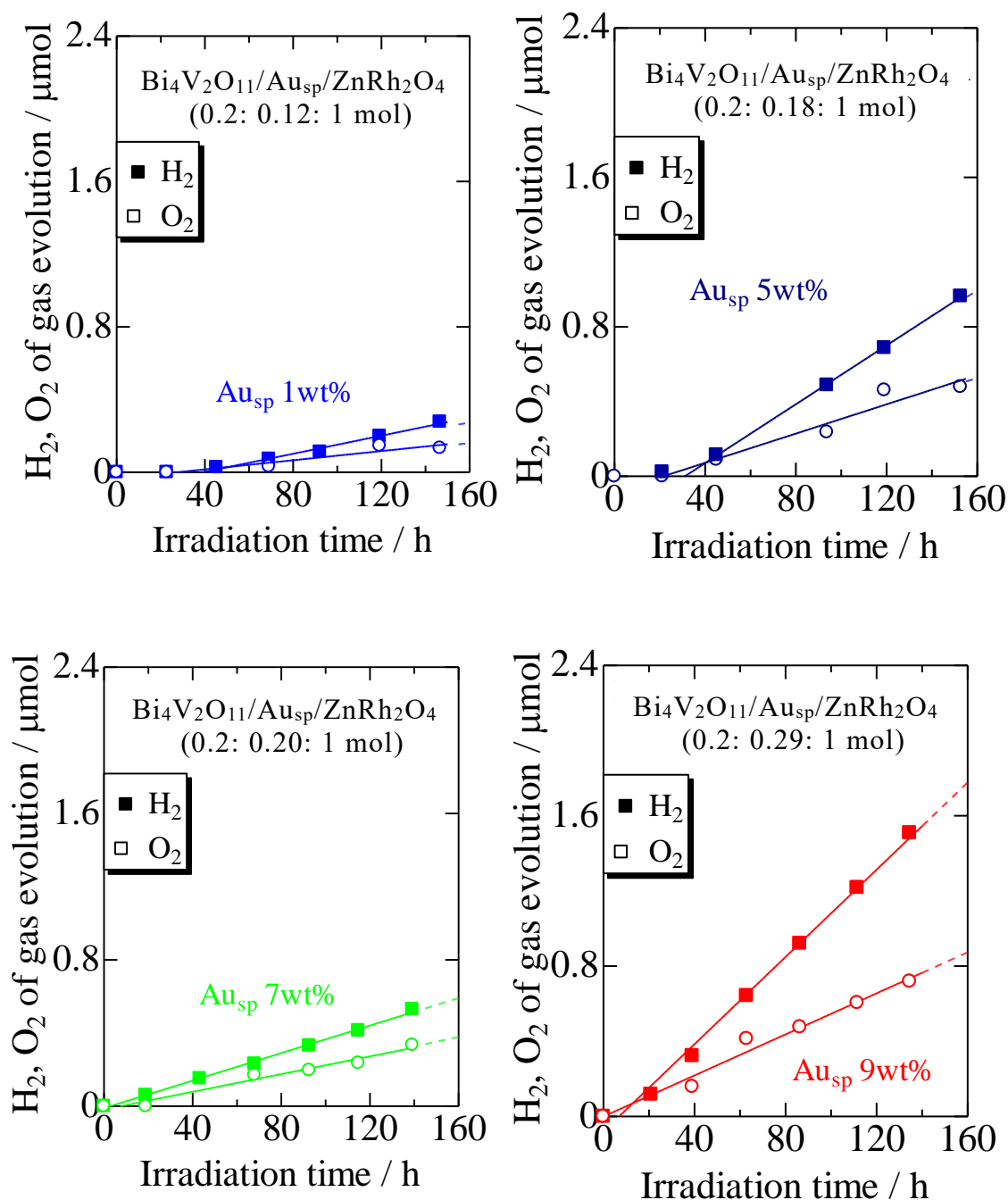


Figure 2.22. XPS quantification results of $\text{Bi}_4\text{V}_2\text{O}_{11}/\text{Au}_{\text{sp}}/\text{ZnRh}_2\text{O}_4/\text{Au}_{\text{sp}}$

2.2.4. Water splitting activity of $\text{Bi}_4\text{V}_2\text{O}_{11}/\text{Au}_{\text{sp}}/\text{ZnRh}_2\text{O}_4/\text{Au}_{\text{sp}}$

Figure 2.23 shows the results of evaluating the water splitting activity of $\text{Bi}_4\text{V}_2\text{O}_{11}/\text{Au}_{\text{sp}}/\text{ZnRh}_2\text{O}_4/\text{Au}_{\text{sp}}$. The compounding ratio was written using the quantified molar ratio of Au. Complete decomposition of pure water was confirmed in all bonded photocatalysts.



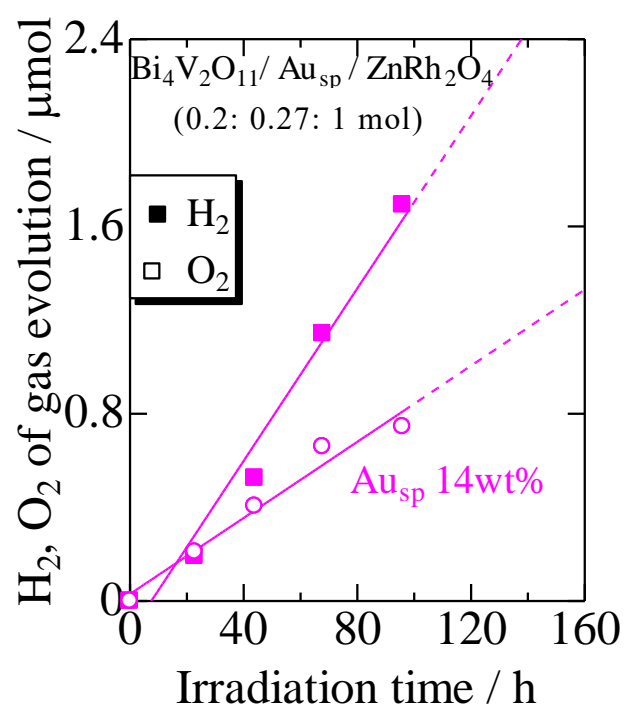


Figure 2.23. Water splitting activity evaluation of Bi₄V₂O₁₁/Au_{sp}/ZnRh₂O₄/Au_{sp}

2.3. Examination of $\text{Bi}_4\text{V}_2\text{O}_{11}/\text{Au}/\text{ZnRh}_2\text{O}_4/\text{Au}$ compounding ratio

Figure 2.24 shows the results for $\text{Bi}_4\text{V}_2\text{O}_{11}/\text{Au}_{\text{com}}/\text{ZnRh}_2\text{O}_4/\text{Au}_{\text{com}}$ and $\text{Bi}_4\text{V}_2\text{O}_{11}/\text{Au}_{\text{sp}}/\text{ZnRh}_2\text{O}_4/\text{Au}_{\text{sp}}$. The ratio of ZnRh_2O_4 (1 mol) and $\text{Bi}_4\text{V}_2\text{O}_{11}$ (0.2 mol) was fixed, and only the compounding ratio of Au was changed.

For $\text{Bi}_4\text{V}_2\text{O}_{11}/\text{Au}_{\text{sp}}/\text{ZnRh}_2\text{O}_4/\text{Au}_{\text{sp}}$, the activity continued to increase up to the maximum amount that could be supported under the experimental conditions, with AQE: 0.015% (0.2:0.27:1mol) showing the highest activity.

However, because the compounding ratio of Au_{sp} could not be optimized, it was not as photocatalytic activity as Au_{com} .

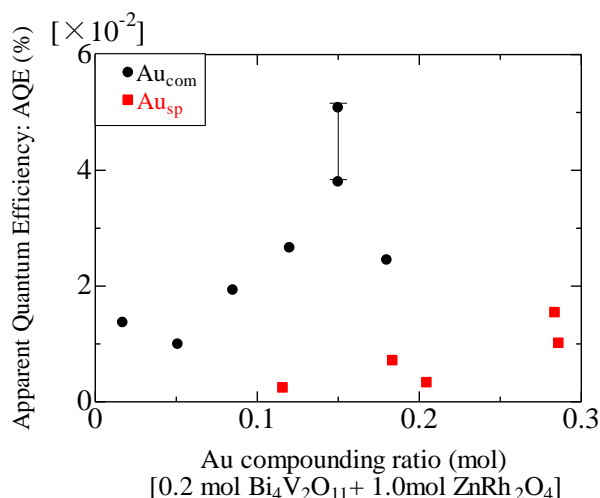


Figure 2.24. AQE comparison of $\text{Bi}_4\text{V}_2\text{O}_{11}/\text{Au}/\text{ZnRh}_2\text{O}_4/\text{Au}$ ($\text{Bi}_4\text{V}_2\text{O}_{11}$: Au: ZnRh_2O_4 = 0.2: x: 1 mol)

Chapter 3. CO₂ reduction by Bi₄V₂O₁₁/Ag/ZnRh₂O₄

3.1. Fabrication and sample evaluation of Bi₄V₂O₁₁/Ag/ZnRh₂O₄

To produce Bi₄V₂O₁₁/Ag/ZnRh₂O₄, silver oxide (Ag₂O) was used as a starting material for Ag, taking advantage of the fact that it is thermally decomposed at 280°C and reduced to metallic Ag. It was also speculated that during the calcination process of Bi₄V₂O₁₁ some amount of Bi₂O₃ was volatilized and the product was a mixture of Bi₄V₂O₁₁ and a small amount of V₂O₅ impurity. In order to remove impurities as much as possible since V₂O₅ reacts with pyrolyzed Ag₂O, the Bi₄V₂O₁₁ powder was soaked and stirred in distilled water for 20 h, followed by filtration and drying at 60 °C for 12 h. Weigh the Bi₄V₂O₁₁ and ZnRh₂O₄ powders prepared in advance together with Ag₂O so that the ratio is Bi₄V₂O₁₁: Ag: ZnRh₂O₄= 1.2: 0.5: 1 (mol) (0.797 g of Bi₄V₂O₁₁, 0.0690 g of Ag₂O, 0.200 g of ZnRh₂O₄), and add acetone. Mixed by ball mill for 20 h. After collecting the sample and forming it into pellets, it was heated at 750°C for 2 hours in an air atmosphere. After pulverizing the calcined pellets into fine powder, the resulting powder was immersed for 5 minutes in 50 mL of a 3 M nitric acid aqueous solution (HNO₃, manufactured by Kanto Kagaku Co., Ltd.) containing approximately 1 g of Bi₄V₂O₁₁/Ag/ZnRh₂O₄. The powder was then thoroughly washed with distilled water and dried at 60°C for 12 hours to obtain Bi₄V₂O₁₁/Ag/ZnRh₂O₄.

The obtained Bi₄V₂O₁₁/Ag/ZnRh₂O₄ powder before and after nitric acid treatment was evaluated by UV-Vis diffuse reflectance spectroscopy and X-ray diffraction analysis. Figure 3.1 shows the XRD pattern of Bi₄V₂O₁₁/Ag/ZnRh₂O₄ powder before and after treatment with nitric acid, and Figure 3.2 shows the UV-Vis diffuse reflectance spectrum. Some unknown peaks were detected in the XRD pattern before HNO₃ treatment, but this is thought to be due to some reaction of V₂O₅ and Ag in Bi₄V₂O₁₁ due to heat treatment (generation of Ag-V composite oxide). On the other hand, most of it was removed after HNO₃ treatment. Furthermore, since the strongest peak of Bi₄V₂O₁₁ (near 28°) relative to the strongest peak of ZnRh₂O₄ also decreased, it is thought that Bi₄V₂O₁₁ also dissolved. The Ag peak could not be confirmed because it overlapped with other peaks before and after heat treatment. The UV-Vis diffuse reflectance spectrum showed an increase in absorption on the long wavelength side (530 nm ≤ λ) before HNO₃ treatment. It is known that the Ag-V complex oxide, which is thought to be produced by the reaction of Ag and Bi₄V₂O₁₁, has a band gap of ~2.2 eV, so this absorption is not attributable to this [21]. Therefore, the increase in absorption is due to the absorption by Ag that is attached to the photocatalyst surface and is not involved in bonding, and since the absorption decreased after HNO₃ treatment, it was thought that the Ag that was attached to the surface and is not involved in bonding was removed.

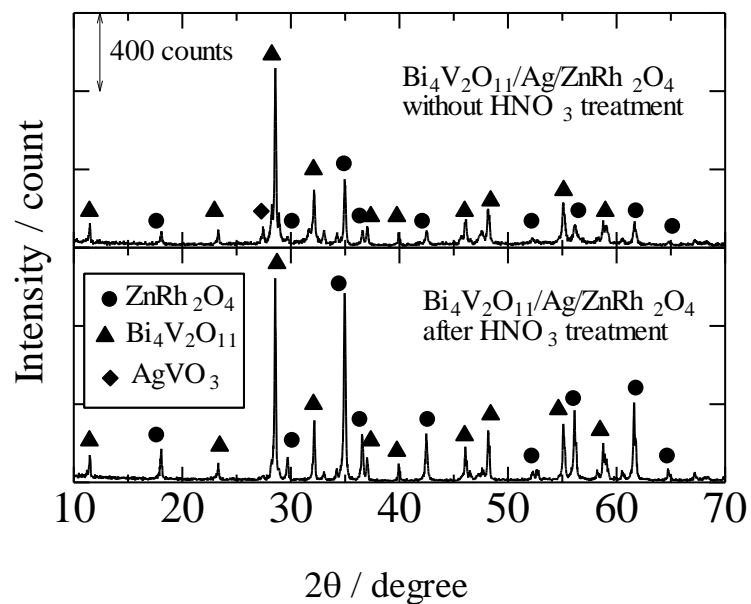


Figure 3.1. XRD pattern of Bi₄V₂O₁₁/Ag/ZnRh₂O₄ before and after nitric acid treatment

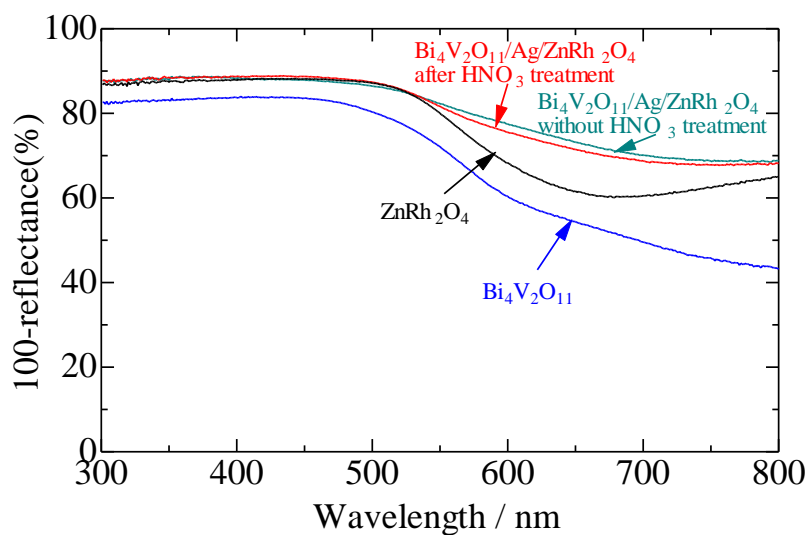


Figure 3.2. UV-Vis diffuse reflectance spectrum of Bi₄V₂O₁₁/Ag/ZnRh₂O₄ after nitric acid treatment

3.2. Selective Cu support by photodeposition on $\text{Bi}_4\text{V}_2\text{O}_{11}/\text{Ag}/\text{ZnRh}_2\text{O}_4$

Since the bandgaps of ZnRh_2O_4 and $\text{Bi}_4\text{V}_2\text{O}_{11}$ are 1.2 eV and 1.7 eV, respectively, when irradiated with light with a wavelength of 850 nm or more, $\text{Bi}_4\text{V}_2\text{O}_{11}$ is not photoexcited, and only ZnRh_2O_4 can be photoexcited, and the co-catalyst can be photodeposited only on ZnRh_2O_4 .

For Cu photodeposition, 80 mg of $\text{Bi}_4\text{V}_2\text{O}_{11}/\text{Ag}/\text{ZnRh}_2\text{O}_4$ was mixed with 10 mL of formaldehyde (HCHO) solution (36.0–38.0%) and 10 mL of 3.15 mM copper (II) acetate monohydrate ($\text{Cu}(\text{CH}_3\text{COO})_2$) as the Cu source. Use a solution of H_2O , Kanto Kagaku, purity >99.0%) dispersed in 30 mL of distilled water. The suspension was then degassed using liquid nitrogen (N_2) and exposed to a light emitting diode (LED) lamp (LEDH60-850; Hamamatsu Photonics) with a wavelength of 850 nm equipped with an optical filter (IR85N; HOYA) for 34 hours. Cu was supported by time photodeposition. This sample was washed with a sufficient amount of distilled water and dried at 60°C.

The results of photodeposition are confirmed by X-ray photoelectron spectroscopy (XPS; Axis-Ultra, Shimadzu) because the amount of particles supported is so small that it cannot be seen from the XRD pattern. The results for Cu are shown in Figures 3.3. The obtained peaks were calibrated using the C 1s peak originating from a hydrocarbon surface contaminant with a binding energy of 284.5 eV. The black line is the bare Z-scheme photocatalyst. Support was confirmed from Cu 2p peaks, but Cu^0 and Cu^+ could not be distinguished, and a satellite peak indicating the presence of CuO was observed.

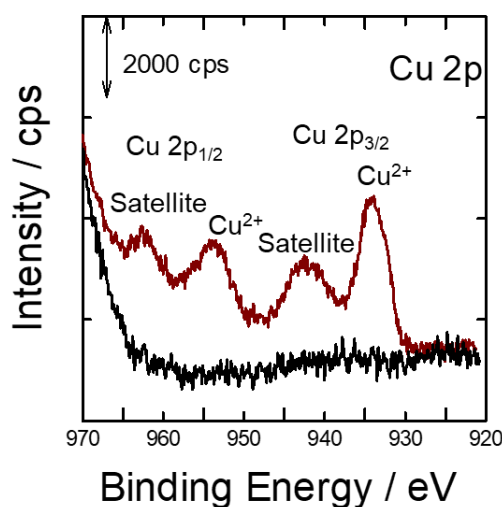


Figure 3.3. Cu 2p before and after Cu loading

Therefore, I applied Auger electron spectroscopy (AES; JAMP-7810, JEOL Ltd.) and X-ray photoelectron spectroscopy (XPS; JPS-9200, JEOL Ltd.) to investigate the Cu valence ratio of photodeposited Cu on the surface. Figure 3.4 shows the AES spectrum (black and white circles) of Cu LMM. The kinetic energies of metallic Cu (CuO state), copper (I) oxide (Cu_2O , Cu^+ state), and copper (II) oxide (CuO , Cu^{2+} state) are reported to be 914.2, 911.8, and 912.6 eV, respectively. Photodeposited Cu may contain not only Cu_2O and CuO but also metallic Cu.

Therefore, the AES spectrum was divided into three peaks fixed at 914.3, 911.7, and 912.7 eV, within ± 0.1 eV of the reported value. Then, when the proportions of Cu, Cu₂O, and CuO were determined from the peak areas, they were 66, 20, and 14 at%, respectively, so Auger analysis showed that Cu⁰ was mainly supported. Additionally, since this AES device does not have an Ar ion etching function, I performed XPS with an Ar ion etching function to measure Cu 2p_{3/2} and Cu 2p_{1/2} and investigate the XPS depth profile (Figure 3.5). By etching the surface, the satellite peak disappears, indicating that CuO exists only on the surface. The satellite peak originated from CuO, decreased when the etching time was 2 min (depth 2 nm from the surface), and disappeared when the etching was extended to 10 min (depth 10 nm). Therefore, CuO exists only in a region up to 10 nm from the surface. Cu and Cu₂O cannot be decomposed because their bond energies are very close, differing by only 0.1 eV. 57 Therefore, I cannot exclude the possibility that Cu₂O exists in the regions where CuO was not detected. However, it can be said that Cu mainly functions as a co-catalyst considering that the reaction is carried out by reduction.

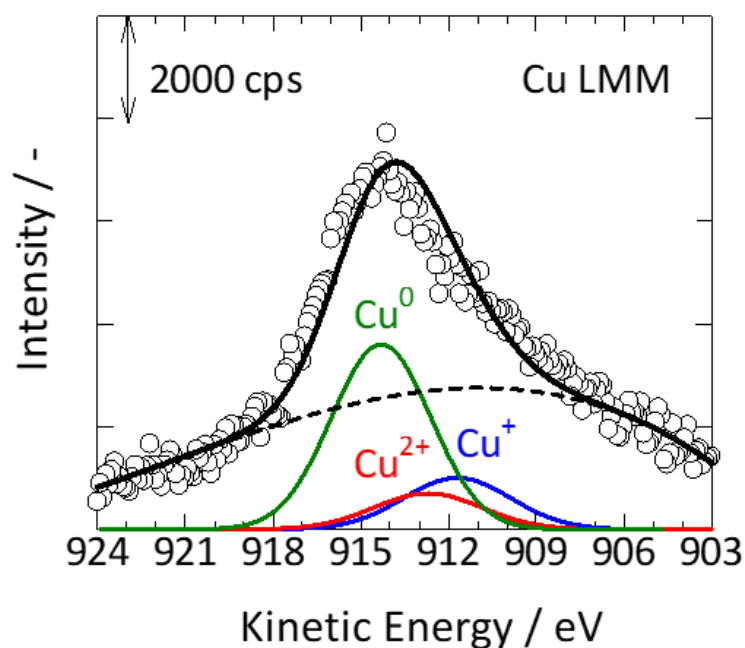


Figure 3.4. AES spectrum of Bi₄V₂O₁₁/Ag/ZnRh₂O₄@Cu

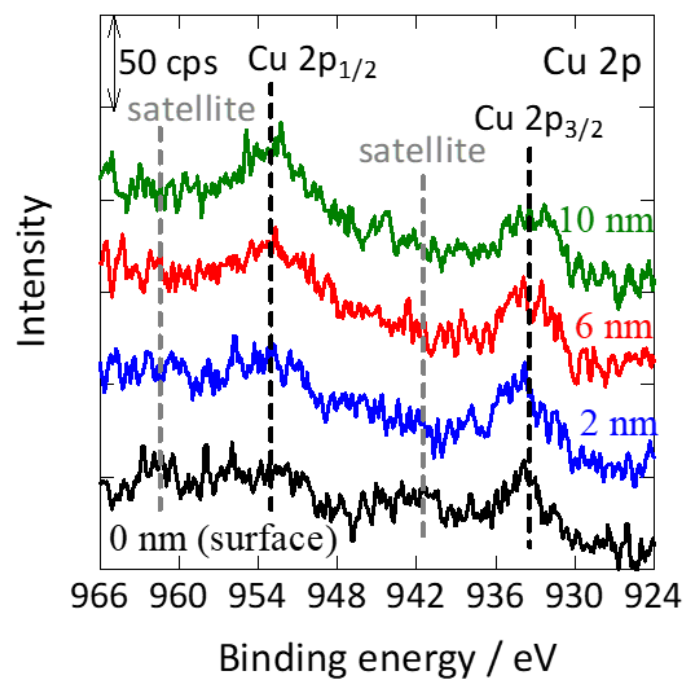


Figure 3.5. XPS spectra of $\text{Bi}_4\text{V}_2\text{O}_{11}/\text{Ag}/\text{ZnRh}_2\text{O}_4@\text{Cu}$ (Etching : 0-10nm)

STEM EDS analysis was performed using scanning transmission electron microscopy (STEM, Tecnai Osiris, FEI) with elemental maps and line maps obtained by energy dispersive X-ray spectroscopy (EDS).

Figure 3.6(b) is the result of line mapping from point A of bismuth vanadate to point B of zinc rhodium oxide in Figure 3.6(a).

In the $\text{Bi}_4\text{V}_2\text{O}_{11}$ at point A, Bi (blue line): V (light blue line) was initially observed at a ratio of 2:1, but Ag (yellow line) appeared in the center and then decreased. Instead, Zn (red line): Rh (wine red line) was observed at a ratio of 1:2 from the middle, and the conductive layer, Ag, decreased. Cu (green line) appeared at the end point of the ZnRh_2O_4 surface. This result confirmed that silver exists as a conductive layer between the two photocatalysts, and Cu exists only on ZnRh_2O_4 .

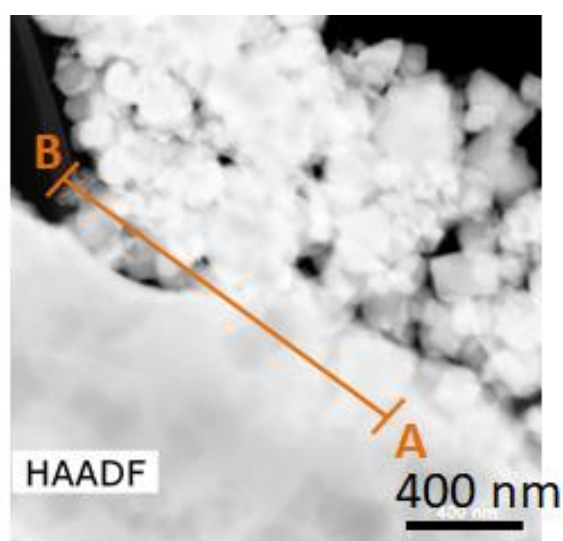


Figure 3.6. (a) HAADF-STEM image of $\text{Bi}_4\text{V}_2\text{O}_{11}/\text{Ag}/\text{ZnRh}_2\text{O}_4@\text{Cu}$

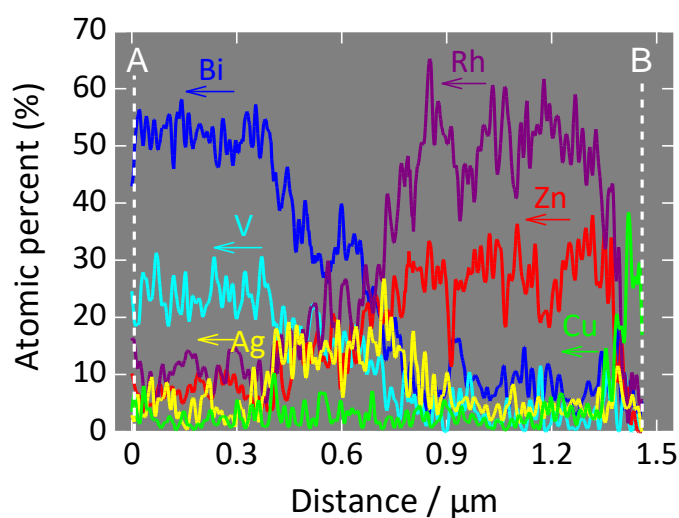


Figure 3.6. (b) Atomic percentages of Bi, V, Ag, Zn, Rh, Cu from $\text{Bi}_4\text{V}_2\text{O}_{11}$ [A] to ZnRh_2O_4 [B]

3.3. Water splitting activity and CO₂ reduction activity of Bi₄V₂O₁₁/Ag/ZnRh₂O₄

Figure 3.7 shows the results of the water splitting activity test of the prepared samples. When water was decomposed under red light with a wavelength of 700 nm, the amount of H₂ and O₂ generated was at a stoichiometric ratio of 2:1, confirming that the complete water decomposition reaction was progressing. The water-splitting activity after photodeposition increased by 3.9 times with the addition of Cu. Its AQE was 0.086%. The CO₂ reduction activity under red light irradiation was evaluated by isotopic analysis using gas mass spectrometry (GCMS), but H₂ could not be detected because Helium gas was used as a carrier, so it was assumed that H₂ was generated due to water oxidation. Water decomposition was confirmed from the amount of O₂ generated.

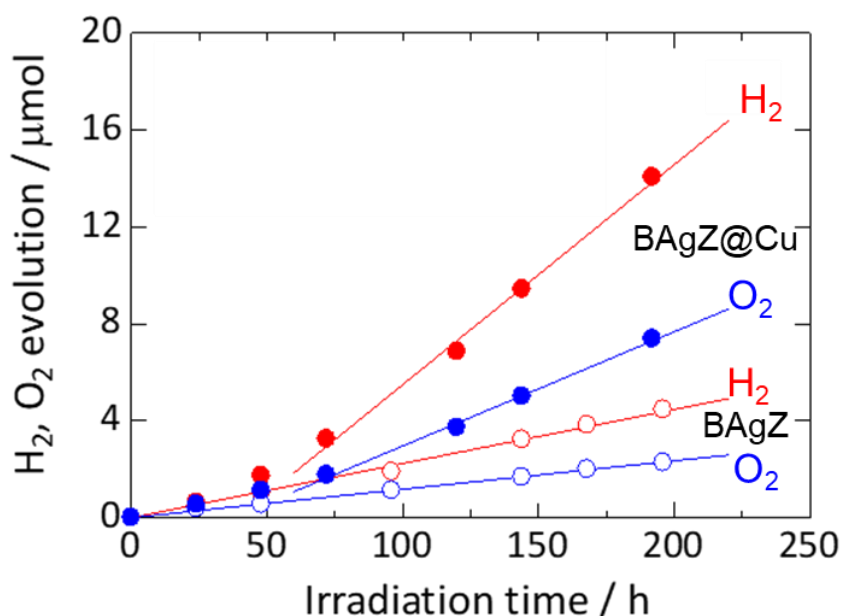


Figure 3.7. Comparison of water splitting activity before and after Cu photodeposition of Bi₄V₂O₁₁/Ag/ZnRh₂O₄

I evaluated the CO₂ reduction activity of Bi₄V₂O₁₁/Ag/ZnRh₂O₄@Cu (Figure 3.8(a)). First, water splitting was confirmed as the same O₂ production rate as in the water splitting test in the absence of CO₂ was obtained. When the atmospheric gas was then changed to ¹³CO₂, the O₂ production rate did not change, but ¹³methane (¹³CH₄) and ¹³carbon monoxide (¹³CO) were newly detected. However, since ¹³CO₂ contains ¹³CO, the possibility of producing CH₄ from CO must be investigated.

Therefore, after confirming reproducibility, I changed the atmospheric gas from ¹³CO₂ to ¹²CO₂, which does not contain CO (Figure 3.8(b)). Similar to the previous Figure 3.8(a), I can see that the rate of O₂ production in these atmospheres is approximately the same as water decomposition. Furthermore, it was confirmed that the activities of CH₄ and O₂ in the ¹³CO₂ atmosphere were the same as before, confirming the reproducibility. In the ¹²CO₂ atmosphere, no CO was detected, but O₂ and CH₄ were detected in an amount that was almost the same as the

activity in the $^{13}\text{CO}_2$ atmosphere. Putting these together, I can see that the generation of CH_4 from CO is ruled out, and that CH_4 is produced by reducing CO_2 using water as an electron source. However, the main reaction is proton reduction, and the amount of CH_4 produced is small, so it is necessary to improve the photocatalytic activity and reduction selectivity. Under these experimental conditions, CO_2 dissolved in water is used for the reaction, so it is considered extremely difficult to reduce CO_2 under the current measurement conditions. Therefore, to improve the selectivity of CO_2 reduction, it is necessary to perform the CO_2 reduction in the gas phase.

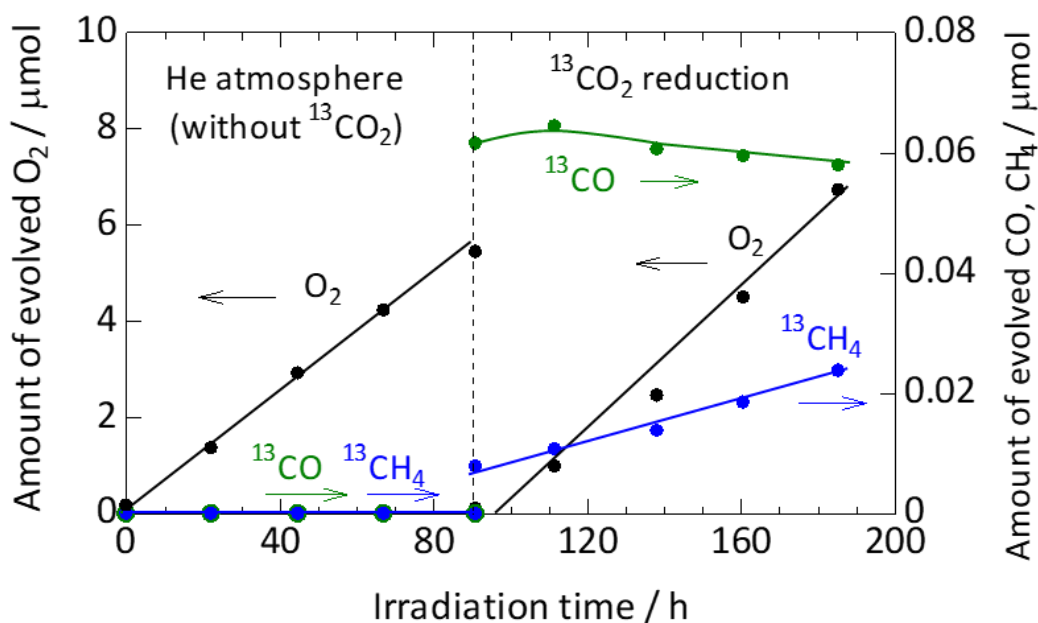


Figure 3.8. (a) CO_2 reduction of $\text{Bi}_4\text{V}_2\text{O}_{11}/\text{Ag}/\text{ZnRh}_2\text{O}_4@\text{Cu}$ in the presence or absence of CO_2

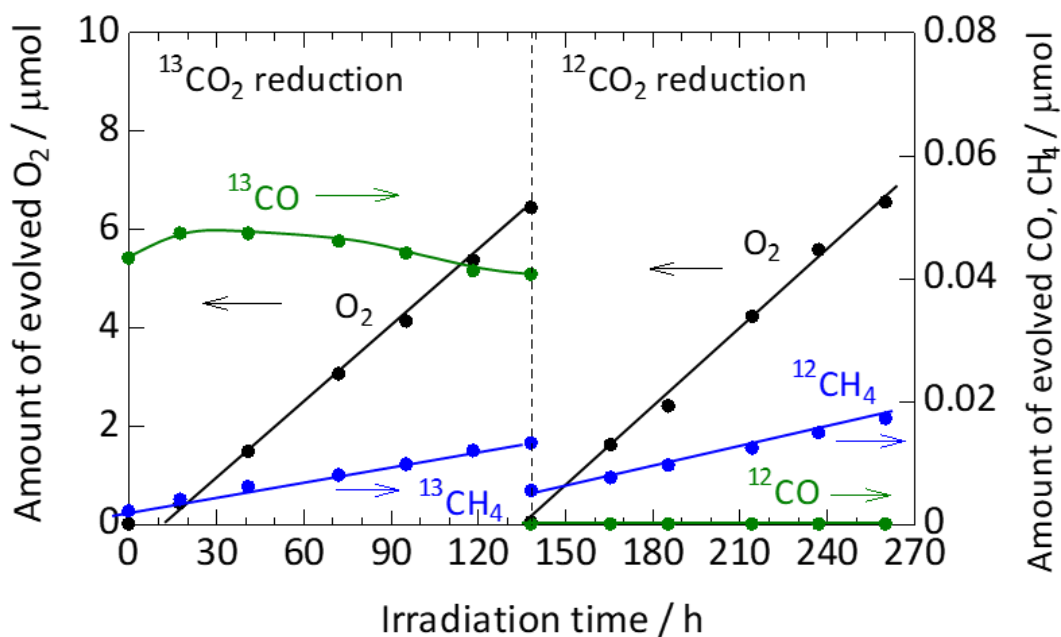


Figure 3.8. (b) CO_2 reduction of $\text{Bi}_4\text{V}_2\text{O}_{11}/\text{Ag}/\text{ZnRh}_2\text{O}_4@\text{Cu}$ in the presence or absence of CO

A CO₂ reduction test was performed on Bi₄V₂O₁₁/Ag/ZnRh₂O₄ to examine the reduction selectivity before Cu loading (Figure 3.9). It was confirmed that the O₂ generation rate was equivalent to the water decomposition rate, and before photodeposition, only CO was generated in a CO₂ atmosphere. Therefore, it can be seen that selective reduction to methane progressed by supporting Cu.

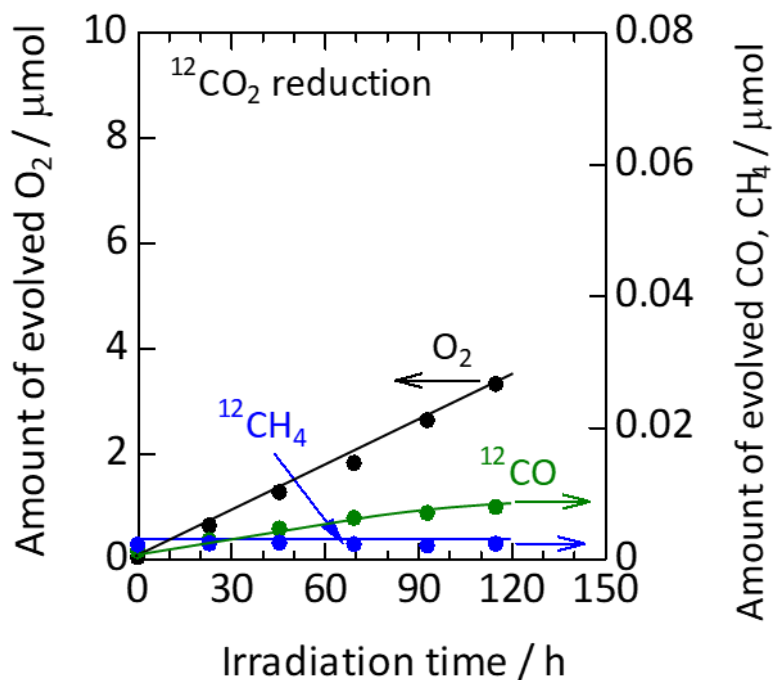


Figure 3.9. Evaluation of CO₂ reduction activity of Bi₄V₂O₁₁/Ag/ZnRh₂O₄ by GCMS

Chapter 4. Social significance and business prospects

4.1. Social significance

As an initiative to address energy and environmental issues, in 2017 Japan began an initiative called the "Hydrogen Strategy ^[34]" to meet domestic demand for H₂ as a new energy alternative to fossil fuels. Japan originally lacked domestic energy resources and was heavily dependent on fossil fuel imports. In addition, the energy self-sufficiency rate further declined due to social anxiety about the safety of nuclear power generation following the Great East Japan Earthquake. For this reason, it has been thought that the use of H₂ can eliminate dependence on fossil fuels without emitting CO₂ during use. However, the original strategy had two major problems ^[35]. One is to aim for a society that uses large amounts of H₂, ignoring the fact that fossil fuels are required as the main method of producing H₂. This has been an ineffective solution to environmental problems and dependence on fossil fuels. Second, there was little investment in technology in the most energy-intensive sectors, such as steel and industry, and subsidies were mainly targeted at very small markets for household goods such as fuel cell cars. These challenges have been compounded by the increased importance of domestic energy stable supply capacity due to subsequent social conditions (coronavirus pandemic, Russia's military invasion of Ukraine), and the hydrogen strategy was revised in June 2023. In addition to the revision, it has been decided to make a large-scale investment of approximately 150 trillion yen over the next 15 years. The new hydrogen strategy aims to use H₂ not only as a new energy resource but also as a raw material, and to achieve carbon neutrality by 2050. At that time, H₂ will not only be cheaper than the current liquefied natural gas (24 yen/Nm³), but also be supplied in large quantities (20 million tons per year), ten times the current amount. To meet these social needs, it is necessary to use renewable energy to produce H₂. Therefore, the practical application of artificial photosynthesis technology using photocatalysts would not only produce H₂ from sunlight and water, but also produce CO and synthetic fuels from H₂ and CO₂ in the presence of CO₂, which would meet the 2050 goal.

4.2. Business prospects

In the commercialization of artificial photosynthesis, research issues include not only photocatalytic activity but also techniques for separating the generated H_2 and O_2 . The water splitting activity of $\text{Bi}_4\text{V}_2\text{O}_{11}/\text{Au}_{\text{com}}/\text{ZnRh}_2\text{O}_4/\text{Au}_{\text{com}}$ in this paper can be improved to about 4% AQE, compared to the practical target AQE= 20%, if the process of activity increase (expansion of reaction vessel, single crystallization of $\text{Bi}_4\text{V}_2\text{O}_{11}$, etc.) discussed in other studies to date is followed. If the activity can be improved by a factor of 5 times, it is possible to reach the target value for practical use. Therefore, the prospects for commercialization are discussed based on the current domestic hydrogen sales price and the target price for 2050.

The commercialization of this system could take the form of a large-scale pool or multiple units that, like solar panels, do not require a factory. Here, I discuss the prospects for the unit-based approach. In this method, as with solar panel power generation, it is necessary to reduce costs both as a unit and as a collective facility. For the unit, it is the activity of the photocatalyst, and for the assembly facility, it is the process from water supply to hydrogen-oxygen separation, except for the optimization of the facility structure. Assuming that the price of H_2 changes from 1200 yen/ kg in 2023 to 222 yen/ kg in 2050, the economic value of H_2 is estimated to increase from 1933 yen/ (year m^{-2}) in 2023 to 358 yen/ (year m^{-2}) in 2050 when AQE= 20% is achieved [34, 36]. Assuming that other necessary costs remain unchanged in 2050, and estimating the cost of 10,000 yen/ (year m^{-2}) for a module with a depreciation period (useful life) of 20 years, a profit of 1,213 yen/ (year m^{-2}) is expected in 2023, but a loss of 280 yen/ (year m^{-2}) is expected in the target value in 2050. The cost of the module is set as approximate because the hydrogen-oxygen separation technology is still in the research stage, and in addition to gas separation using membranes, the Z-scheme photocatalyst may be used to physically separate the products by separating the conductive layers. Therefore, in order to meet the final goal of 2050, it is necessary to improve photocatalytic activity and lower the cost of the module to meet the price of hydrogen supply. The prospects for this include progress in basic research (improvement of catalyst life, higher activity, and cost reduction of modules such as gas separation technology) and government subsidies, which will effectively make it feasible to commercialize the technology.

On the other hand, the selectivity and activity of CO_2 reduction have not yet achieved realistic values for commercialization. Therefore, as a future prospect, it may be possible to use fine metal particles prepared by sputtering into an ionic liquid as a CO_2 reduction co-catalyst in order to increase CO_2 reduction selectivity. The advantage of this method is that it is easy to refine the alloy regardless of the type of metal. Therefore, I believe that it can be used to design excellent CO_2 reduction cocatalysts. Furthermore, since the evaluation was conducted on CO_2 reduction in a liquid phase with an excess of water, which is a proton source, I believe that more CO_2 reduction products can be obtained by changing the reaction phase to a gas phase.

Chapter 5. Conclusions

5.1. Conclusions

To summarize the water splitting of $\text{Bi}_4\text{V}_2\text{O}_{11}/\text{Au}_{\text{com}}/\text{ZnRh}_2\text{O}_4/\text{Au}_{\text{com}}$, I optimized the composition ratio and found that $\text{Bi}_4\text{V}_2\text{O}_{11}:\text{Au}_{\text{com}}:\text{ZnRh}_2\text{O}_4 = 0.2:0.15:1$ was optimal, so I changed this Au ratio in the next miniaturization investigation. Using a sputtering film-forming method conducted in collaboration with Professor Torimoto, the Au particles used in the conductive layer were miniaturized, and the final bonded sample was 50 nm, one-tenth of the conventional size. Furthermore, when the compounding ratio of $\text{Bi}_4\text{V}_2\text{O}_{11}/\text{Au}_{\text{sp}}/\text{ZnRh}_2\text{O}_4/\text{Au}_{\text{sp}}$ was varied, complete water splitting was confirmed in all samples, as the ratio of H_2 and O_2 was 2:1 under red light irradiation. This confirmed that Au_{sp} functions as a conductive layer without any problems. Although the activity continued to improve up to the maximum amount that could be supported under the experimental conditions, the optimal value could not be found. Finally, the optimum value (AQE: 0.051%) was confirmed at a compounding ratio of $\text{Bi}_4\text{V}_2\text{O}_{11}:\text{Au}_{\text{com}}:\text{ZnRh}_2\text{O}_4 = 0.2:0.15:1$.

To summarize the CO_2 reduction of $\text{Bi}_4\text{V}_2\text{O}_{11}/\text{Ag}/\text{ZnRh}_2\text{O}_4/\text{Cu}$, isotope analysis by GCMS revealed that the water splitting activity does not change even in a CO_2 atmosphere, and CH_4 is produced by reduction of CO_2 and oxidation of water under red light irradiation. It was confirmed that the selectivity for reducing CO_2 to CH_4 was improved by supporting Cu. However, since proton reduction is still the main reaction, it is necessary to improve the activity and selectivity of CO_2 reduction.

In the Z-scheme photocatalyst, the charges not used in the reaction are consumed in the conductive layer. Normally, I would like to use all of the excited electrons and holes, but if I can use a photocatalyst that responds to the entire spectrum of visible light, as I used here, I can ultimately increase the number of usable photons. The cocatalyst not only improves photocatalytic activity but also plays an important role in controlling reduction selectivity in CO_2 reduction. The sputtering method used in this study allows for the production of not only various metals but also alloys, which is expected to be applied to CO_2 reduction research. It is hoped that the knowledge obtained in this study on the use of fine metals as conductive layers will be useful in this research. I suspect that by doing so, I can achieve realistic activity for commercialization in CO_2 reduction as well.

【References】

- [1] *Journal of the Hydrogen Energy Systems Society of Japan*, 2008, Vol.33, No.2
- [2] A. Fujishima, K. Honda, *Nature*, 1972, 238, 37
- [3] K. Sayama and H. Arakawa, *J. Phys. Chem.*, 1993, 97, 531.
- [4] K. Yamaguchi, and S. Sato, *J. Chem. Soc., Faraday Trans. 1*, 1985, 81, 1237
- [5] A. Kudo, K. Domen, K. Maruya and T. Onishi, *Chem. Phys. Lett.*, 1987, 133, 517.
- [6] D. E. Scaife, *Solar energy*, 25, 41 (1980)
- [7] K. Maeda, K. Teramura, D. Lu, T. Takata, N. Saito, Y. Inoue and K. Domen, *Nature*, 2006, 440, 295
- [8] Y. Lee, H. Terashima, Y. Shimodaira, K. Teramura, M. Hara, H. Kobayashi, K. Domen and M. Yashima, *J. Phys. Chem. C*, 2007, 111, 1042
- [9] H. Liu, J. Yuan, W. Shangguan and Y. Teraoka, *J. Phys. Chem. C*, 2008, 112, 8521
- [10] N. Lei, M. Tanabe and H. Irie, *Chem. Commun.*, 2013, 49, 10094.
- [11] P. Dhanasekaran and N. M. Gupta, *Int. J. Hydrogen Energy*, 2012, 37, 4897.
- [12] R. Asai, H. Nemoto, Q. Jia, K. Saito, A. Iwase and A. Kudo, *Chem. Commun.*, 2014, 50, 2543
- [13] C. Pan, T. Takata, M. Nakabayashi, T. Matsumoto, N. Shibata, Y. Ikumura and K. Domen, *Angew. Chem., Int. Ed.*, 2015, 54, 2955.
- [14] J. Liu, Y. Liu, N. Liu, Y. Han, X. Zhang, H. Huang, Y. Lifshitz, S. T. Lee, J. Zhong and Z. Kang, *Science*, 2015, 347, 970.
- [15] Q. Wang, M. Nakabayashi, T. Hisatomi, S. Sun, S. Akiyama, Z. Wang, Z. Pan, X. Xiao, T. Watanabe, T. Yamada, N. Shibata, T. Takata, K. Domen, *Nat. Mater* 2019, 18, 827.
- [16] K. Sayama, K. Mukasa, R. Abe, Y. Abe and H. Arakawa, *J. Photochem. Photobiol., A*, 2002, 148, 71.
- [17] H. Kato, M. Hori, R. Kato, Y. Shimodaira, A. Kudo, *Chem. Lett.*, 2004, 33, 1348.
- [18] A. Iwase, Y. H. Ng, Y. Ishiguro, A. Kudo and R. Amal, *J. Am. Chem. Soc.*, 2011, 133, 11054.
- [19] Y. Sasaki, H. Nemoto, K. Saito and A. Kudo, *J. Phys. Chem. C*, 2009, 113, 17536.
- [20] K. Iwashina, A. Iwase, Y. H. Ng, R. Amal, A. Kudo, *J. Am. Chem. Soc.*, 2015, 137, 604.
- [21] R. Kobayashi, T. Takashima, S. Tanigawa, S. Takeuchi, B. Ohtani, H. Irie, *Phys. Chem. Chem. Phys.*, 2016, 18, 27693
- [22] K. Kamijyo, T. Takashima, M. Yoda, J. Osaki, H. Irie, *Chem. Commun.*, 2018, 54, 7999-8002
- [23] Y. Negishi, Y. Matsuura, R. Tomizawa, W. Kurashige, Y. Niihori, T. Takayama, A. Iwase and A. Kudo, *J. Phys. Chem. C*, 2015, 119 (20), 11224-11232
- [24] J.-C. Wang, H.-C. Yao, Z.-Y. Fan, L. Zhang, J.-S. Wang, S.-Q. Zang, Z.-J. Li, *ACS Appl. Mater. Interfaces* 2016, 8, 3765.
- [25] S. Tonda, S. Kumar, M. Bhardwaj, P. Yadav, S. Ogale, *ACS Appl. Mater. Interfaces*, 2018, 10, 2667.
- [26] S. Yoshino, T. Takayama, Y. Yamaguchi, A. Iwase, A. Kudo, *J. Am. Chem. Soc.* 2022, 144, 2323.
- [27] S. Higuchi, T. Takashima, J. Osaki, H. Irie, *Catal. Today*, 2019, 335, 402.
- [28] K. Maeda, K. Domen, *J. Phys. Chem. Lett.*, 2010, 1, 2655
- [29] T. Torimoto, K. Okazaki, T. Kiyama, K. Hirahara, N. Tanaka, and S. Kuwabata, *Appl. Phys. Lett.*, 2006, 89, 243117
- [30] Y. Takimoto, T. Kitta, H. Irie, *Int. J. Hydrogen Energy*, 2012, 37, 134.

- [31] F. Abraham, M. F. Debreuille-Gresse, G. Mairesse, G. Nowogrocki, *Solid State Ionics.*, 1988, 28-30, 529.
- [32] V. M. Zainullina, V. M. Zhukovskii, E. S. Buyanova, Y. V. Emel'yanova, *J. Inorg. Chem.*, 2007, 52, 225.
- [33] V. Thakral, S. Uma, *Mater. Res. Bull.*, 2010, 45, 1250.
- [34] Japan, Basic Hydrogen Strategy, Jun. 6, 2023.
- [35] Renewable energy institute, Re-examining Japan's Hydrogen Strategy Moving Beyond the "Hydrogen Society" Fantasy, Sept. 22, 2023.
- [36] T. Setoyama, Artificial photosynthesis process technology development Consideration of project results and achievement status Future prospects (Translate from Japanese), NEDO Artificial Photosynthesis Project Public Results Report Meeting Materials, Jan. 25, 2022.

【Acknowledgment】

First and foremost, I would like to express my sincere gratitude to my supervisor, Professor Hiroshi Irie, for his appropriate advice and enthusiastic guidance during the implementation of this research. I would also like to express my sincere gratitude to everyone in the laboratory for their cooperation in various ways. I would like to express my sincere gratitude to Professor Tsukasa Torimoto for his willingness to undertake joint research and for his careful guidance.